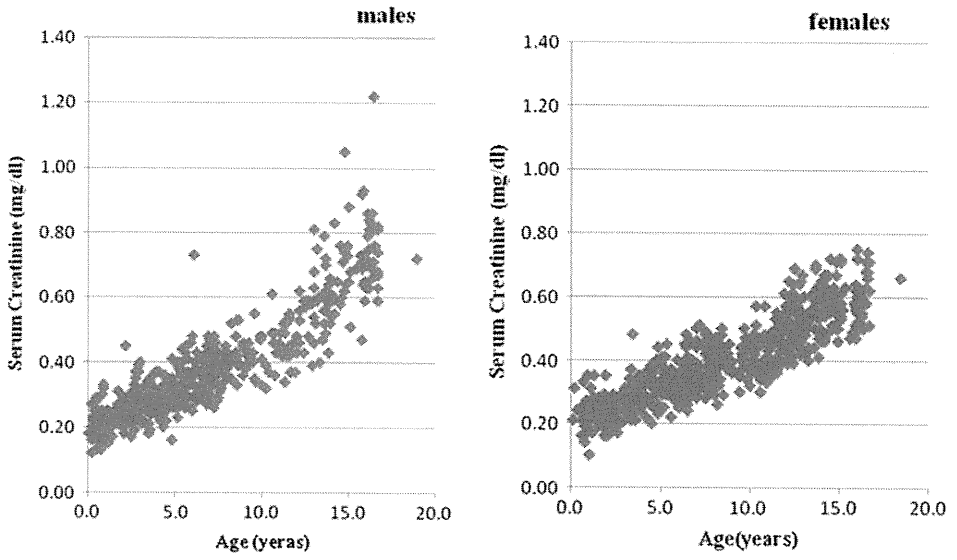

Fig. 1 Correlations between serum Cr concentration and age in all subjects divided according to sex. These scattergrams show that reference serum Cr concentration gradually increases with age, and the increase is more marked in males than females in adolescence

Table 1 Median, 2.5 percentile, and 97.5 percentile of serum Cr reference value in each age group regardless of sex between 3 months and 11 years old

Age	*N*	2.5%	50.0%	97.5%
3–5 months	18	0.14	0.20	0.26
6–8 months	19	0.14	0.22	0.31
9–11 months	31	0.14	0.22	0.34
1 year	70	0.16	0.23	0.32
2 years	73	0.17	0.24	0.37
3 years	88	0.21	0.27	0.37
4 years	81	0.20	0.30	0.40
5 years	96	0.25	0.34	0.45
6 years	102	0.25	0.34	0.48
7 years	85	0.28	0.37	0.49
8 years	56	0.29	0.40	0.53
9 years	36	0.34	0.41	0.51
10 years	44	0.30	0.41	0.57
11 years	58	0.35	0.45	0.58

(Table 2). The median reference value in males was almost equal to that in females at the age of 12 years; however, the median reference value in males increased rapidly, and became significantly different from that in females at 16 years old (0.73 mg/dl and 0.59 mg/dl, respectively, $P < 0.0001$).

We reviewed the median, 2.5 percentile, and 97.5 percentile of serum Cr reference values in each body length group in males and females (Table 3). We again found that the median reference values were higher in males than in females >160 cm in body length.

The correlations between serum Cr value and body length were determined in subjects aged 2–11 years. The regression equation was $y = 0.34x$–0.044, and that passing through the origin was $y = 0.30x$. A significant positive correlation was observed in 717 children aged 2–11 years, with a correlation coefficient of 0.732 (Fig. 2, $P < 0.001$).

Table 2 Median, 2.5 percentile, and 97.5 percentile of reference serum Cr value between 12- and 16-year-old males and females

Sex	Males				Females			
Age (years)	*n*	2.5%	50.0%	97.5%	*n*	2.5%	50.0%	97.5%
12	15	0.40	0.53	0.61	54	0.40	0.52	0.66
13	30	0.42	0.59	0.80	38	0.41	0.53	0.69
14	17	0.54	0.65	0.96	40	0.46	0.58	0.71
15	15	0.48	0.68	0.93	22	0.47	0.56	0.72
16	30	0.62	0.73	0.96	27	0.51	0.59	0.74

In all subjects, the relationships between body length and serum Cr level were determined by polynomial regression analysis in males and females, and reference serum Cr level was expressed as a quintic equation of body length (Figs. 3, 4). The regression equations were $y = -1.259x^5 + 7.815x^4 - 18.57x^3 + 21.39x^2 - 11.71x + 2.628$ in 516 males, and $y = -4.536x^5 + 27.16x^4 - 63.47x^3 + 72.43x^2 - 40.06x + 8.778$ in 630 females. Significant correlations were observed in males with a correlation coefficient of 0.908 (Fig. 3, $P < 0.001$), and in females with a correlation coefficient of 0.879 (Fig. 4, $P < 0.001$).

Discussion

GFR is used to assess kidney function, and is measured by renal clearance techniques. Inulin clearance is the gold standard for evaluation of kidney function, but cannot be measured easily. Therefore, various methods to determine GFR have been used. One method involves monitoring

Table 3 Median, 2.5 percentile, and 97.5 percentile of reference serum Cr value in each body length group in males and females

Sex	Males				Females			
Body length (cm)	*n*	2.5%	50.0%	97.5%	*n*	2.5%	50.0%	97.5%
<70	30	0.13	0.20	0.29	9	0.14	0.23	0.25
≥70 to <80	33	0.15	0.22	0.34	34	0.15	0.23	0.35
≥80 to <90	44	0.18	0.23	0.35	44	0.17	0.24	0.29
≥90 to <100	58	0.19	0.27	0.38	49	0.20	0.27	0.37
≥100 to <110	67	0.20	0.30	0.42	72	0.24	0.32	0.42
≥110 to <120	77	0.26	0.36	0.47	102	0.25	0.34	0.46
≥120 to <130	45	0.28	0.40	0.53	50	0.28	0.39	0.49
≥130 to <140	31	0.33	0.41	0.54	34	0.31	0.42	0.52
≥140 to <150	25	0.34	0.49	0.61	55	0.31	0.45	0.64
≥150 to <160	30	0.41	0.56	0.93	132	0.39	0.55	0.72
≥160 to <170 (≥160 in females)	48	0.46	0.67	0.86	49	0.47	0.58	0.68
≥ 170	28	0.57	0.72	1.02				

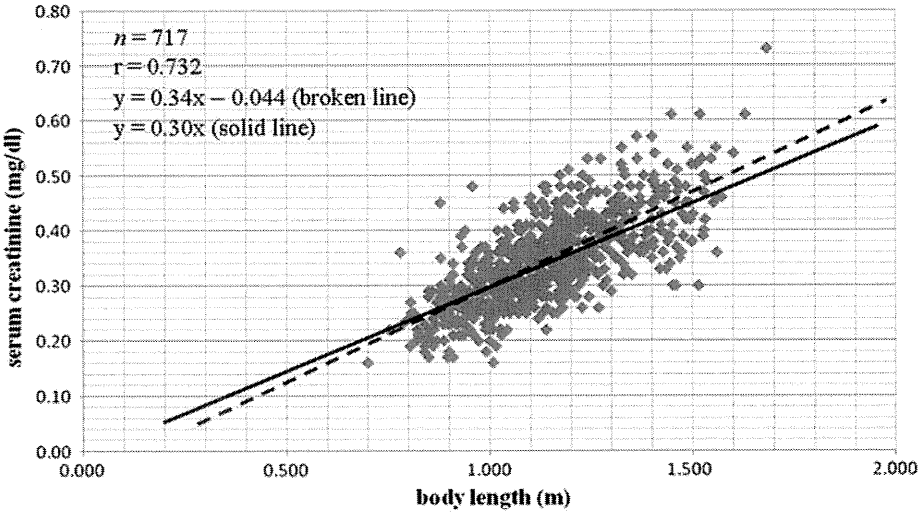

Fig. 2 Correlations between serum Cr values and body length (2–11 years). The regression equation was $y = 0.34x–0.044$, and that passing through the origin was $y = 0.30x$. A significant positive correlation was observed in 717 children aged 2–11 years, with a correlation coefficient of 0.732 ($P < 0.001$)

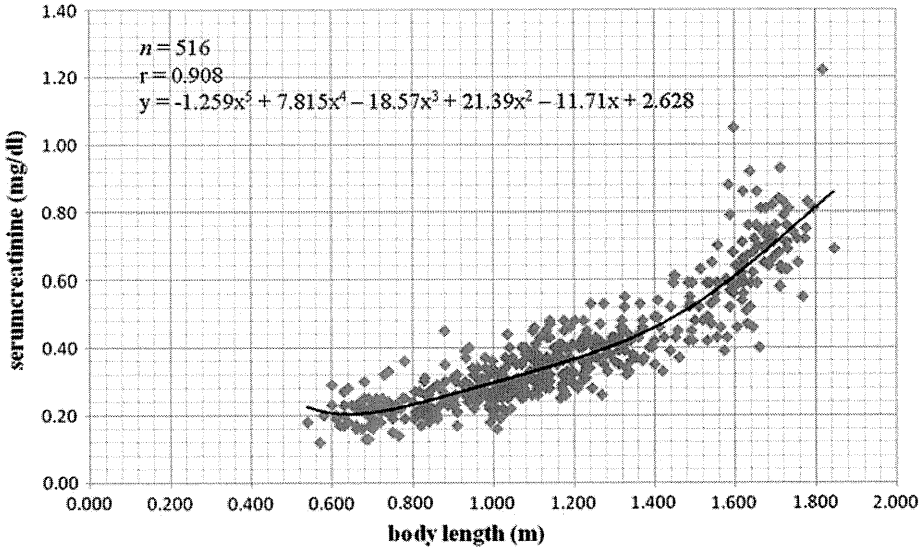

Fig. 3 Correlations between serum Cr value and body length (males, 3 months–18 years). A significant correlation between serum Cr value and body length was determined by polynomial regression analysis in males, and reference serum Cr level was expressed as a quintic equation of body length

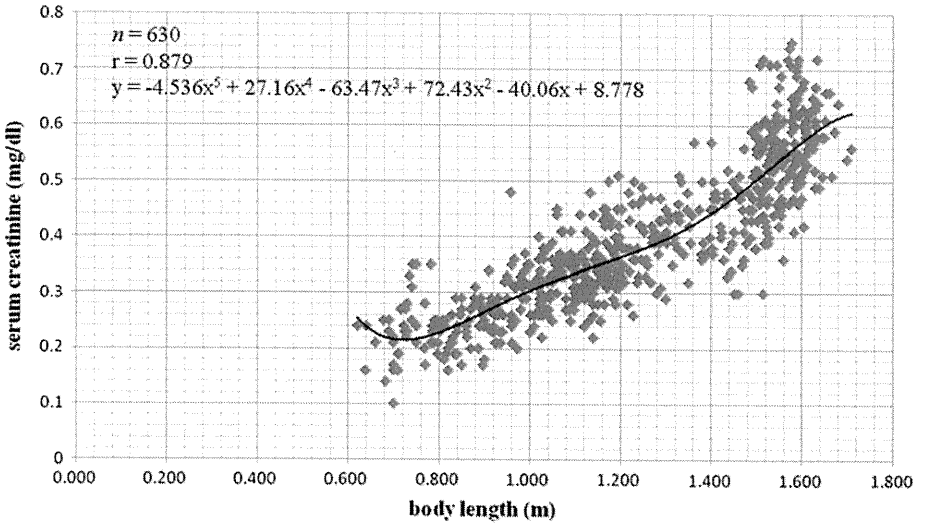

Fig. 4 Correlations between serum Cr value and body length (females, 3 months–18 years). A significant correlation between serum Cr value and body length was determined by polynomial regression analysis in females, and reference serum Cr level was expressed as a quintic equation of body length

endogenous Cr clearance, but tubular secretion of Cr can result in overestimation of GFR. The eGFR ((ml/min/1.73 m^2) = κ × body length (cm)/serum Cr value (mg/dl)) by the Jaffe method devised by Schwartz [1] has been used clinically. More recently, however, enzymatic methods have been used to measure Cr rather than the Jaffe method, so we cannot use the formula in this form. Therefore, it was necessary to re-evaluate the value of the coefficient κ in the formula. Recently, Zappitelli et al. [7] revised the Schwartz formula relating eGFR to serum Cr level determined enzymatically, and they reported that the κ value in the Schwartz equation decreased from 0.55 to 0.47 for children and adolescent girls. Schwartz reported the updated formula as eGFR = 0.413 × body length (cm)/serum Cr value (mg/dl) by the enzymatic method showing a 25% reduction in κ value from the previous value of 0.55 generated from Jaffe-based serum Cr measurements [5]. Counahan et al. [8] generated a similar formula using 'near-true' Cr determination measured by the Jaffe method after removal of non-Cr chromogen with ion-exchange resin, in children of varying ages, and the resulting κ was 0.43.

We have presented the correlations between serum Cr concentration and age by scattergrams in Fig. 1. The results indicated that reference serum Cr concentrations increase gradually with age, and the increase is more marked in males than females in adolescence. This was thought to be because muscle mass increases more rapidly in males than in females. Serum Cr reference values for each age and sex makes it possible for clinical laboratories to determine whether patients have normal renal function or not without the need to obtain height information in pediatric patients. Therefore, we reviewed the median, 2.5 percentile, and 97.5 percentile of serum Cr reference values for each age and sex (Tables 1, 2). We can use 0.30 mg/dl at the age of 4 years and 0.41 mg/dl at the age of 10 years as reference median serum Cr values to investigate renal function in children. The median reference value in males was almost equal to that in females at the age of 12 years; however, the median reference value became higher in males than in females, based on both age and body length, and became significantly higher in males than in females at age 16 years due to sex-related differences in muscle mass in adolescence. Tanaka et al. [9] reported reference intervals of serum Cr value based on an enzymatic method in Japanese children by a latent reference value extraction method. Their reference data were slightly higher than those in the present study, because they could not completely exclude cases with mild renal dysfunction.

When we transform the formula of Schwarz, the normal serum Cr will be proportional to body length: normal serum Cr value (mg/dl) = κ × body length (m). Therefore, we determined the correlation between body length and serum Cr value by an enzymatic method and determined the coefficient k of the regression equation. A significant positive correlation with correlation coefficient > 0.7 was found in Japanese children aged 2–11 years. In addition, the differences in Cr value when we substituted the minimal and the maximal variables of body length in the two types of regression equation, i.e., the conventional equation and the equation passing through the origin were < 0.025 mg/dl in each group. Therefore, we used the regression equation that passed through the origin for all children aged 2–11 years, taking clinical usefulness into account, i.e., body length (m) × 0.30 yielded a value similar to the reference serum Cr level in Japanese children aged 2–11 years. This formula is equivalent to that reported previously in a single-center study in Japanese children aged 1–12 years [6].

In all subjects, the relationship between body length and serum Cr level was determined by polynomial regression analysis separately in males and females, and the reference

serum Cr level was expressed as a quintic equation of body length with highly significant correlations. As the reciprocal of serum Cr is generally correlated with GFR [1–5, 8] we could utilize the equation for eGFR derived from serum Cr, eGFR (%) = (reference serum Cr/patient's serum Cr) × 100. Assuming a GFR with 100% equal to GFR with 120 ml/min/1.73 m^2, we derived the equation eGFR (ml/min/1.73 m^2) = (reference serum Cr/patient's serum Cr) × 120. This means that it is likely that the eGFR based on the Schwartz formula will be expressed by the quintic equation instead of a linear equation of body length in Japanese children of all ages. Studies for standardization of inulin clearance in Japanese children and to develop formulae for estimation of GFR are currently underway, but large-scale studies are not possible because of the small numbers of pediatric CKD patients. Therefore, our equations may become a useful tool to support these investigations.

The correlations between age and body length were determined in all subjects and a significant positive correlation was observed with a correlation coefficient of 0.974. Therefore, due to their multicollinearity, we have not analyzed serum Cr by a multiple regression model with age and height as covariants.

Reference serum Cr levels expressed as the median, 2.5 percentile, and 97.5 percentile are useful for pediatricians to determine whether a patient shows normal renal function. Our formula, derived from body length in Japanese children aged 2–11 years, yielded reference serum Cr levels to evaluate renal function in pediatric CKD patients that are simple and easy to use. In addition, our quintic equations, derived from body length in Japanese children of all ages, will be useful to estimate their renal function, despite the complicated formulae, since computerization of medical care simplifies application of these formulae. Since we were unable to validate our equations using a different dataset, our future work will include efforts to validate these equations. Nevertheless, we consider that these reference serum Cr levels will be applicable for screening of renal function in Asian as well as Japanese children; these methods of evaluating renal function in children are available worldwide.

Acknowledgments This study was financially supported by the Kidney Foundation, Japan. We thank Midori Awazu, MD, Takashi Sekine, MD, Mayumi Sako, MD, Takuji Yamada, MD, Yuko Akioka, MD, and Hirotsugu Kitayama, MD, of the Committee of Measures for Pediatric CKD, for their contributions to the improvement of this manuscript.

References

1. Schwartz GJ, Brion LP, Spitzer A. The use of plasma creatinine concentration for estimating glomerular filtration rate in infants, children, and adolescents. Pediatr Clin North Am. 1987;34:571–90.
2. Schwartz GJ, Feld LG, Langford DJ. A simple estimate of glomerular filtration rate in full-term infants during the first year of life. J Pediatr. 1984;104:849–54.
3. Schwartz GJ, Haycock GB, Edelmann CM Jr, Spitzer A. A simple estimate of glomerular filtration rate in children derived from body length and plasma creatinine. Pediatrics. 1976;58:259–63.
4. Schwartz GJ, Gauthier B. A simple estimate of glomerular filtration rate in adolescent boys. J Pediatr. 1985;106:522–6.
5. Schwartz GJ, Muñoz A, Schneider MF, Mak RH, Kaskel F, Warady BA, Furth SL. New equations to estimate GFR in children with CKD. J Am Soc Nephrol. 2009;20:629–37.
6. Uemura O, Ushijima K, Nagai T, Yamada T, Hayakawa H, Shinkai Y, Kuwabara M. Reference serum creatinine levels determined by an enzymatic method in Japanese children: relationship to body length. Clin Exp Nephrol. 2009;13:585–8.
7. Zappitelli M, Parvex P, Joseph L, Paradis G, Grey V, Lau S, Bell L. Derivation and validation of cystatin C-based prediction equations for GFR in children. Am J Kidney Dis. 2006;48:221–30.
8. Counahan R, Chantler C, Ghazali S, Kirkwood B, Rose F, Barratt TM. Estimation of glomerular filtration rate from plasma creatinine concentration in children. Arch Dis Child. 1976;51:875–8.
9. Tanaka T, Yamashita A, Ichihara K. Reference intervals of clinical tests in children determined by a latent reference value extraction method. J Jpn Pediatr Soc. 2008;112:1117–32. (in Japanese).

Am J Physiol Renal Physiol 300: F873–F886, 2011.
First published January 12, 2011; doi:10.1152/ajprenal.00503.2010.

Amelioration of renal alterations in obese type 2 diabetic mice by vasohibin-1, a negative feedback regulator of angiogenesis

Daisuke Saito,[1] Yohei Maeshima,[1] Tatsuyo Nasu,[1] Hiroko Yamasaki,[1] Katsuyuki Tanabe,[1] Hitoshi Sugiyama,[1,2] Hikaru Sonoda,[3] Yasufumi Sato,[4] and Hirofumi Makino[1]

[1]*Department of Medicine and Clinical Science,* [2]*Center for Chronic Kidney Disease and Peritoneal Dialysis, Okayama University Graduate School of Medicine, Dentistry and Pharmaceutical Sciences, Okayama;* [3]*Discovery Research Laboratories, Shionogi, Osaka; and* [4]*Department of Vascular Biology, Institute of Development, Aging, and Cancer, Tohoku University, Sendai, Japan*

Submitted 26 August 2010; accepted in final form 9 January 2011

Saito D, Maeshima Y, Nasu T, Yamasaki H, Tanabe K, Sugiyama H, Sonoda H, Sato Y, Makino H. Amelioration of renal alterations in obese type 2 diabetic mice by vasohibin-1, a negative feedback regulator of angiogenesis. *Am J Physiol Renal Physiol* 300: F873–F886, 2011. First published January 12, 2011; doi:10.1152/ajprenal.00503.2010.—The involvement of VEGF-A as well as the therapeutic efficacy of angiogenesis inhibitors in diabetic nephropathy have been reported. We recently reported the therapeutic effects of vasohibin-1 (VASH-1), an endogenous angiogenesis inhibitor, in a type 1 diabetic nephropathy model (Nasu T, Maeshima Y, Kinomura M, Hirokoshi-Kawahara K, Tanabe K, Sugiyama H, Sonoda H, Sato Y, Makino H. *Diabetes* 58: 2365–2375, 2009). In this study, we investigated the therapeutic efficacy of VASH-1 on renal alterations in obese mice with type 2 diabetes. Diabetic *db/db* mice received intravenous injections of adenoviral vectors encoding human VASH-1 (AdhVASH-1) and were euthanized 8 wk later. AdhVASH-1 treatment resulted in significant suppression of glomerular hypertrophy, glomerular hyperfiltration, albuminuria, increase in the $CD31^+$ glomerular endothelial area, $F4/80^+$ monocyte/macrophage infiltration, the accumulation of type IV collagen, and mesangial matrix. An increase in the renal levels of VEGF-A, VEGFR-2, transforming growth factor (TGF)-β1, and monocyte chemoattractant protein-1 in diabetic animals was significantly suppressed by AdhVASH-1 (immunoblotting). AdhVASH-1 treatment significantly recovered the loss and altered the distribution patterns of nephrin and zonula occludens (ZO)-1 and suppressed the increase in the number of fibroblast-specific protein-1 ($FSP\text{-}1^+$) and $desmin^+$ podocytes in diabetic mice. In vitro, recombinant human VASH-1 (rhVASH-1) dose dependently suppressed the upregulation of VEGF induced by high ambient glucose (25 mM) in cultured mouse podocytes. In addition, rhVASH-1 significantly recovered the mRNA levels of nephrin and the protein levels of ZO-1 and P-cadherin and suppressed the increase in protein levels of desmin, FSP-1, Snail, and Slug in podocytes under high-glucose condition. Taken together, these results suggest the potential use of VASH-1 as a novel therapeutic agent in type 2 diabetic nephropathy mediated via antiangiogenic effects and maintenance of podocyte phenotype in association with antiproteinuric effects.

podocyte; proteinuria

DIABETIC NEPHROPATHY IS COMPLICATED in 30–40% of patients with type 2 diabetes and is the most common pathological disorder predisposing end-stage renal disease in Japan and the Western world. Glomerular hyperfiltration, glomerular and tubular hypertrophy, microalbuminuria, and thickening of the glomerular basement membrane (GBM) are observed in the early stage of diabetic nephropathy. Then, expansion of the mesangial extracellular matrix (ECM) and overt proteinuria are observed, eventually leading to glomerulosclerosis and tubulointerstitial fibrosis (27). The involvement of various factors and cytokines including the renin-angiotensin-aldosterone system, oxidative stress, insulin-like growth factor-I, monocyte chemoattractant protein-1 (MCP-1), transforming growth factor-β1 (TGF-β1), protein kinase C and advanced glycation end products (AGE) in diabetic nephropathy has been reported (4, 36).

Angiogenesis is associated with a number of pathological conditions including tumor growth and diabetic retinopathy (13). Vascular endothelial growth factor-A (VEGF-A), a potent stimulator of angiogenesis, promotes endothelial cell proliferation, migration, and endothelial cell tube formation (11) and also induces vascular permeability (9).

Previous studies have demonstrated an increased glomerular filtration surface area in diabetic nephropathy in association with the formation of new glomerular capillaries (14, 30) and a slight elongation of the preexisting capillaries (14, 30), analogous to the changes in pathological diabetic retinopathy (25). In addition, the increase in the levels of VEGF-A and the receptor of VEGF-A, VEGFR-2, has been reported in diabetic nephropathy models (7, 41). The therapeutic efficacies of anti-VEGF-A strategies (i.e., neutralizing antibodies and a receptor tyrosine kinase inhibitor) (8, 12, 38) as well as amelioration of diabetic glomerular alterations in mice with inducible podocyte-specific overexpression of soluble flt-1, an antagonist of VEGF-A (21). have further demonstrated the potential involvement of VEGF-A in the progression of diabetic nephropathy.

Recently, the therapeutic effects of angiogenesis inhibitors such as tumstatin peptide, endostatin peptide, angiostatin, pigment epithelium derived factor (PEDF), and NM-3 (17, 18, 25, 43, 48, 50) in diabetic nephropathy models have been reported by others and us.

Vasohibin-1 (VASH-1), an endogenous angiogenesis inhibitor, was identified from a microarray analysis assessing genes upregulated by VEGF-A in endothelial cells (45). Human VASH-1 protein is composed of 365 amino acid residues (45). VASH-1 is induced by representative angiogenic factors such as VEGF-A and fibroblast growth factor 2 (FGF-2) (45). VASH-1 regulates proliferation and migration of endothelial cells in an autocrine manner and thus is considered to serve as a negative feedback regulator of angiogenesis. In addition, VASH-1 inhibits lymphangiogenesis and lymph node metastasis of tumors (16). VASH-1 does not contain a classic signal

Address for reprint requests and other correspondence: Y. Maeshima, Dept. of Medicine and Clinical Science, Okayama Univ. Graduate School of Medicine and Dentistry, 2-5-1 Shikata-cho, Okayama, 700-8558, Japan (e-mail: ymaeshim@md.okayama-u.ac.jp).

sequence, and a small vasohibin-binding protein (SVBP) serves as a secretory chaperon for VASH-1 and contributes to the antiangiogenic effects of VASH-1 (39). To date, cell surface receptors for VASH-1 have not been reported. The therapeutic efficacies of VASH-1 on tumor growth, atherosclerosis, and proliferative retinopathy models have been reported (37, 45, 49). We recently reported the therapeutic effects of adenoviral transfer of VASH-1 (AdhVASH-1) in a mouse type 1 diabetic nephropathy model (29). Renoprotective effects of VASH-1 were mediated via its direct effects on mesangial cells as well as glomerular endothelial cells, suggesting the ability of VASH-1 beyond the "antiangiogenic factor."

Nephrin, a glomerular podocyte protein, is crucial for maintaining the integrity of the interpodocyte slit membrane structure and an intact filtration barrier. In diabetic nephropathy, loss of intact podocyte-specific expression patterns of slit membrane-associated proteins such as nephrin (2), zonula occludin (ZO)-1, P-cadherin, and the expression of mesenchymal markers such as desmin, fibroblast-specific protein-1 (FSP-1) as well as Snail, a transcription factor involved in epithelial-to-mesenchymal transition (EMT), in association with the loss of glomerular filtration barrier function, has been reported (22, 47).

In the present study, we demonstrate the therapeutic efficacy of VASH-1 in ameliorating renal alterations in type 2 diabetic *db/db* mice. Treatment with AdhVASH-1 markedly suppressed characteristic alterations of diabetic nephropathy without affecting metabolic parameters. These effects were associated with the regulation of VEGF-A signals, inhibitory effects on chemokine and the direct protective effects of VASH-1 on podocytes, potentially leading to the amelioration of albuminuria.

MATERIALS AND METHODS

Adenoviral vectors. A replication-defective adenoviral vector encoding human VASH-1 was prepared as previously described (45). A replication-defective adenovirus vector encoding the *Escherichia coli* β-galactosidase (AdLacZ), which is identical to AdhVasohibin-1 (AdhVASH-1), except for the inserted cDNA, was used as the control (45). Adenoviral vectors were expanded in human embryonic kidney cell line 293 and purified by cesium chloride ultracentrifugation as described previously (19). The purified viruses were dialyzed against PBS with 10% glycerol and stored at −70°C until use. The viral concentration and the viral titer were determined as previously described (45).

Experimental protocols. The experimental protocol was approved by the Animal Ethics Review Committee of Okayama University. Adult male *db/db* mice (BKS.Cg-*db/db* Jcl; Clea Japan, Osaka, Japan) and their age-matched nondiabetic *db/m* littermates (BKS.Cg-*db/+m* Jcl; Clea Japan) were used. Mice were fed a standard pellet laboratory chow and were provided with water ad libitum. The *db/db* mice were included in this study at the age of 8 wk since they develop hyperglycemia at 7–8 wk of age(6). At the age of 8 wk, the blood glucose of *db/db* mice was in the range of 19.4–26.2 mmol/l. Mice were divided into four subgroups (n = 6/subgroup): *1*) nondiabetic-control db/m mice and *db/db* mice treated either with *2*) vehicle buffer (saline), *3*) AdLacZ, or *4*) AdhVASH-1. Adenoviral vectors (AdLacZ or AdhVASH-1) or saline (via tail veins) were intravenously injected using a syringe with a 27-gauge needle and were repeatedly injected every other week (7.5×10^9 vp/100 μl). Eight weeks following the initial injections of adenoviral vectors, the mice were euthanized and the kidneys were obtained. The optimal viral titer for the present experiments was determined following preliminary in vivo experiments with various titers of AdhVASH-1, and the titer as described was utilized since we could confirm the increase in VASH-1 levels in sera after 2 wk as detected by the immunoblots (data not shown).

Blood glucose was monitored every week. No mice died, and no signs of apparent exhaustion were observed during the experimental period. At 0 and 8 wk after initiation of the intravenous injection of adenoviral vectors, the body weight and the individual 24-h food consumption were measured. At 8 wk after initiation of treatment, individual 24-h urine sample collection was performed using metabolic cages. Nonfasting blood samples were drawn from the retroorbital venous plexus using heparinized capillary tubes under anesthesia at the time of euthanasia. Kidney, liver, and heart weight was measured just after euthanasia.

Blood and urine examination. Blood glucose was measured in tail-vein blood, and urine was tested for ketone bodies and glucose by Okayama Medical Laboratories (Okayama, Japan). Serum and urinary creatinine levels were measured by HPLC. Urinary albumin concentration was measured by ELISA (Bethyl Laboratories, Montgomery, TX) following the manufacturer's instructions. Results were normalized to the urinary creatinine levels and expressed as the urinary albumin/creatinine ratio (UACR). The creatinine clearance (Ccr) was calculated and expressed as milliliters per minute per 100 grams of body weight. Serum levels of mouse insulin were determined by ELISA using an ultrasensitive rat insulin ELISA kit and mouse insulin standard (Morinaga, Yokohama, Japan) following the manufacturer's instructions. According to the manufacturer's technical information, mouse insulin can be measured in combination with a mouse insulin standard due to a high homology among mammalian animals. All samples were examined in duplicate, and mean values of individual sera were utilized for statistical analysis. The intra- and interassay coefficients of variation for the insulin assays were <5% and <10%, respectively.

Measurement of blood pressure. Arterial blood pressure was measured before euthanasia using a programmable sphygmomanometer (BP-98A; Softron, Tokyo, Japan) by the tail-cuff method as described previously (15).

Histological analysis. At 8 wk after the start of treatment, the kidneys were removed, fixed in 10% buffered formalin, and embedded in paraffin. Sections (4-μm) were stained with periodic acid-Schiff for light microscopic observation. The mean glomerular tuft volume (G_V) was determined from the mean glomerular cross-sectional tuft area (G_A) as described previously (17, 46, 48) Twenty glomeruli from each cortical area were observed, images were taken and analyzed by using Lumina Vision software (Mitani, Fukui, Japan) to determine the mean G_A. G_V was calculated as $G_V = \beta/k \times (G_A)^{3/2}$, with $\beta = 1.38$, the shape coefficient for spheres, and $k = 1.1$, a size distribution coefficient (46).

The mesangial matrix index was defined as the proportion of the glomerular tuft occupied by the mesangial matrix, excluding nuclei. The mesangial matrix areas of 20 glomeruli in each kidney were analyzed and averaged. The mesangial areas were selected using Photoshop software (Adobe Systems, San Jose, CA), followed by analysis using Lumina Vision.

Immunohistochemistry. Immunofluorescence staining of CD31, type IV collagen, nephrin, and zonula occludens (ZO)-1 was performed using frozen sections as previously described (17, 29). The following antibodies were used as primary antibodies: a rat anti-mouse CD31 monoclonal antibody (Pharmingen, San Diego, CA); polyclonal rabbit anti-mouse type IV collagen antibody (Chemicon International, Temecula, CA); polyclonal guinea pig anti-nephrin antibody (Fitzgerald, Concord, MA); and polyclonal rabbit anti-zonula occludens (ZO)-1 antibody (Zymed Laboratories, Carlsbad, CA). Briefly, frozen sections (4-μm) were fixed in cold (−10°C) acetone for 10 min and then air dried. The sections were blocked with 10% normal goat serum (Sigma, St. Louis, MO) for CD31, type IV collagen, and nephrin or Protein Block Serum-Free (Dako Cytomation, Carpinteria, CA) for ZO-1. The sections were incubated with

primary antibodies as described above for 1 h. Then, the sections were washed, and incubated with secondary antibodies for 30 min at room temperature. After washing in PBS, sections were observed by a confocal laser fluorescence microscope (LSM-510; Carl Zeiss, Jena, Germany). The following FITC-conjugated antibodies were used as secondary antibodies: Alexa Fluor 546-labeled goat anti-rat IgG (CD31, Invitrogen, Carlsbad, CA); Alexa Fluor 488-labeled anti-rabbit IgG (type IV collagen and ZO-1, Invitrogen); and Alexa Fluor 488-labeled anti-guinea pig IgG (nephrin, Invitrogen).

The immunoreactivity of glomerular CD31 or type IV collagen was quantified as follows; color images were obtained as TIF files by LSM-510. The brightness of each image file was analyzed using

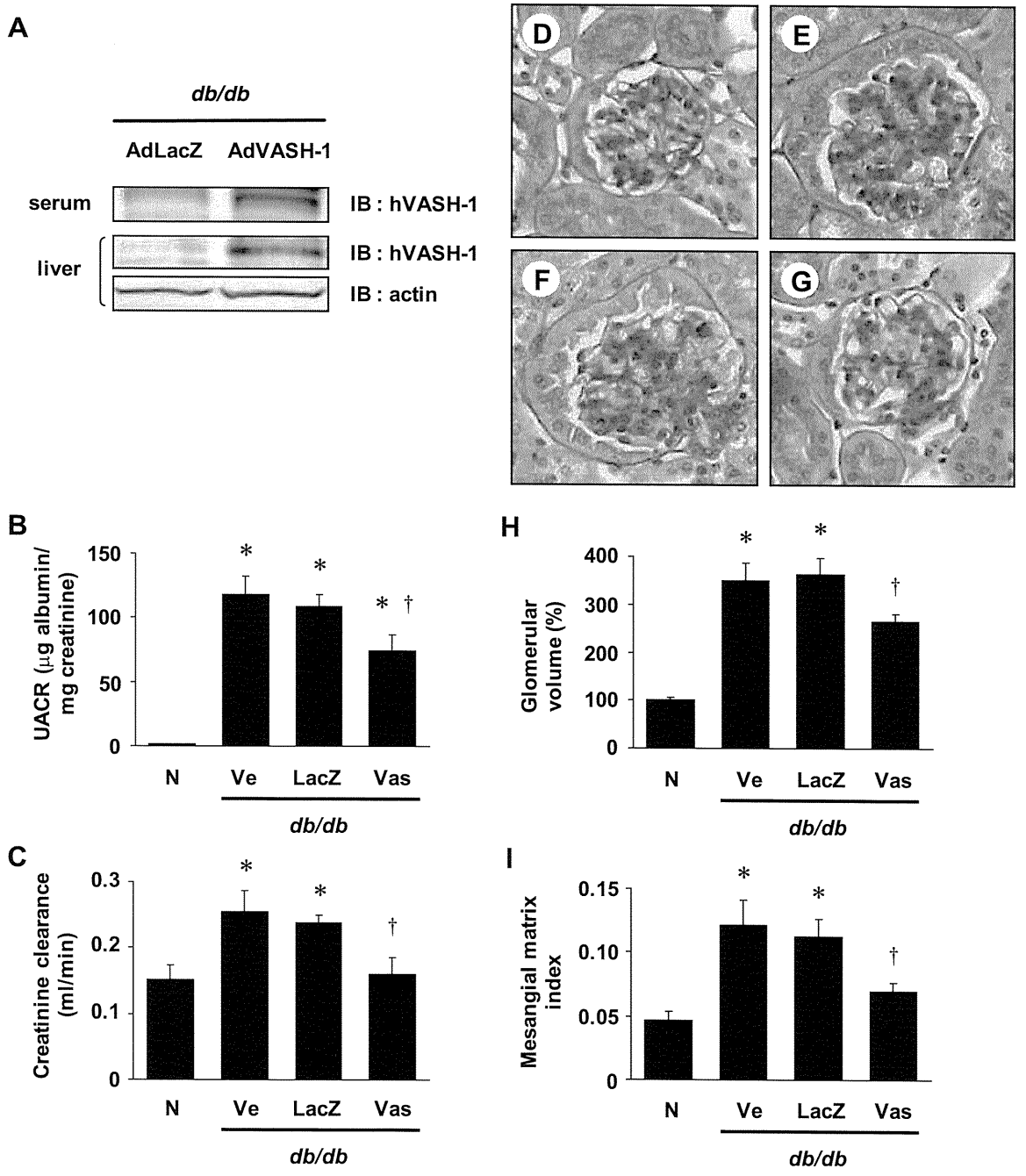

Fig. 1. *A*: immunoblot analysis. Immunoblots for human vasohibin-1 (VASH-1) and actin are shown. Each lane was loaded with 25 μg protein obtained from the serum samples or liver. Adenoviral vector (AdhVASH-1)-injected *db/db* mice exhibited significantly elevated serum VASH-1 (42 kDa) levels compared with the AdLacZ-injected *db/db* mice (16 wk of age). Similarly, enhanced protein levels of VASH-1 in the liver were observed in AdhVASH-1-treated mice compared with AdLacZ-treated *db/db* mice. Immunoblots for actin are shown to confirm equal loading. *B*: increase in urinary albumin/creatinine ratio (UACR) in *db/db* mice was significantly suppressed by treatment with AdhVASH-1 (Vas; 16 wk of age). $*P < 0.05$ vs. *db/m*. $\dagger P < 0.05$ vs. *db/db* mice treated with vehicle buffer (Ve) or *db/db* mice treated with AdLacZ (LacZ). *C*: increase in creatinine clearance (Ccr) in *db/db* mice was partially suppressed by AdhVASH-1 (16 wk of age). $*P < 0.05$ vs. *db/m*. $\dagger P < 0.05$ vs. Ve or LacZ. *D–G*: representative light microscopic appearance of glomeruli (periodic acid-Schiff staining; original magnification ×400) for *db/m* mice (*D*), *db/db* mice treated with either vehicle buffer (*E*), AdLacZ (*F*), or AdhVASH-1 (*G*) at 16 wk of age. *H*: increase in glomerular volume in *db/db* mice was diminished by treatment with AdhVASH-1. *I*: mesangial matrix index was defined as the proportion of the glomerular tuft occupied by the mesangial matrix area (excluding nuclei). Each column consists of means ± SE. $*P < 0.01$ vs. *db/m*. $\dagger P < 0.05$ vs. Ve or LacZ; $n = 6$/group.

Table 1. *Body weight, blood glucose concentration, and food consumption*

Group	Week 0			Week 8		
	Body Weight, g	Blood Glucose, mmol/l	Food Consumption, g/24 h	Body Weight, g	Blood Glucose, mmol/l	Food Consumption, g/24 h
Nondiabetic	26.7 ± 0.3	6.5 ± 0.1	3.0 ± 0.6	31.2 ± 1.0	6.6 ± 0.4	3.4 ± 0.1
Diabetic (vehicle)	39.4 ± 0.2*	23.3 ± 0.8*	6.2 ± 0.2*	50.8 ± 1.3*	25.8 ± 0.9*	6.2 ± 0.1*
Diabetic (Ad-LacZ)	39.8 ± 0.5*	23.3 ± 1.1*	6.2 ± 0.1*	50.1 ± 1.9*	26.0 ± 0.9*	6.0 ± 0.3*
Diabetic (Ad-VASH-1)	40.0 ± 0.3*	23.1 ± 0.5*	6.0 ± 0.3*	51.0 ± 1.0*	25.2 ± 1.2*	5.9 ± 0.3*

Values are means ± SE; n = 6/group. Vehicle; vehicle buffer-treated; VASH-1, vasohibin-1. *$P < 0.01$ vs. nondiabetic controls.

Lumina Vision. Image files (TIF) were inverted and opened in grayscale mode. Type IV collagen or CD31 indices were calculated using the following formula, {[X (density) × positive area (μm^2)]/ glomerular total area (μm^2)}, where the staining density is indicated by a number from 0 to 256 in grayscale. In regard to peritubular capillary (PTC) density, the number of $CD31^+$ peritubular capillaries in each high-power field was determined. The PTC density of 20 high-power fields in each kidney was analyzed and averaged.

To evaluate the staining pattern of nephrin and ZO-1, the following "re-distribution" score was used as described by Macconi et al. (24). A score was assigned to each individual glomerulus in the tissue section. The score 0, 0.5, and 1.0 were used, respectively, for continuous distribution along the glomerular capillary wall, heterogeneous distribution along the glomerular membrane (with variable staining intensity from one region to another within the same glomerulus), and markedly discontinuous distribution. The final score per section was then calculated as the weighted mean: score = $(N_1 \times 0 + N_2 \times 0.5 + N_3 \times 1)/(N_1 + N_2 + N_3)$, where N_i (i = 1–3) is the number of glomeruli in each category.

Glomerular accumulation of monocytes/macrophages was determined by immunohistochemistry using rat anti-mouse F4/80 antibody (Serotec, Oxford, UK). Frozen sections were fixed in acetone for 10 min and exposed to H_2O_2 to eliminate endogenous peroxidase activity. The kidney sections were then blocked with 10% goat serum for 30 min and incubated with a primary antibody for 60 min. The sections were then washed with PBS and exposed to a secondary antibody, horseradish peroxidase (HRP)-labeled goat anti-rat IgG (Chemicon) for 1 h. Diaminobenzidine was used as a chromogen. The number of $F4/80^+$ cells was determined by observing >20 glomeruli from each section. All slides were counterstained with hematoxylin. Normal rat IgG was used as a negative control.

For immunohistochemistry of desmin and FSP-1, formalin (10%)-fixed, paraffin-embedded sections (4-μm) were used. After deparaffinization, sections were incubated with goat polyclonal anti-desmin antibody (Santa Cruz Biotechnology, Santa Cruz, CA) or rabbit polyclonal anti-S100A4 (FSP-1) antibody (Dako Cytomation) followed by incubation with biotinylated secondary antibody, and immunoperoxidase staining was carried out utilizing a Vectastain ABC Elite reagent kit (Vector Labs, Burlingame, CA) as previously described (18, 48). Diaminobenzidine was used as a chromogen. The number of desmin or $FSP\text{-}1^+$ cells (podocytes) was determined by observing >30 glomeruli from each section. All slides were counterstained with hematoxylin. Normal goat IgG was used as a negative control.

Western blotting. Briefly, kidneys or liver was homogenized in radioimmunoprecipitation assay (RIPA) Lysis buffer (Santa Cruz Biotechnology) at 4°C. Similarly, cultured podocytes were lysed using RIPA buffer as previously described (17, 26). After centrifugation at 13,000 rpm for 30 min at 4°C, supernatant was collected and stored at −80°C until use. Total protein concentration was determined by using a DC-protein determination system (Bio-Rad Laboratories) using BSA as a standard. Samples were processed for SDS-PAGE, and proteins were electrotransferred onto nitrocellulose membranes with iBlot Dry Blotting System (Invitrogen). The membranes were blocked with 5% nonfat dry milk in 1× TBS (0.1% Tween 20) for 1 h, incubated overnight with polyclonal rabbit anti-mouse TGF-β1/2/3 (Santa Cruz Biotechnology), polyclonal rabbit anti-VEGF-A, anti-VEGFR-2 (Santa Cruz Biotechnology), hamster anti-mouse MCP-1 (BioLegend, San Diego, CA), monoclonal anti-human VASH-1 (45), or polyclonal rabbit anti-mouse VASH-1 (37) antibodies at 4°C. After incubation with HRP-labeled secondary antibodies for 1 h, signals were detected with the ECL system (Amersham). Membranes were reprobed with rabbit polyclonal anti-actin antibodies (Bio-Rad) to serve as controls for equal loading. The density of each band was determined by using Image J software and expressed as a value relative to the density of a corresponding band obtained from actin immunoblot.

Recombinant VASH-1. Recombinant human VASH-1 was prepared as previously described (45). Human VASH-1 protein connected to the FLAG tag at the C terminus was expressed in a Bac-to-Bac baculovirus expression system (Life Technologies, Tokyo, Japan) according to the manufacturer's instructions and purified as a soluble protein (45).

Cell culture. Conditionally immortalized mouse podocytes, generous gifts from Prof. Peter Mundel (University of Miami Miller School of Medicine, Miami, FL), were cultured on type I collagen-coated flasks (BD Falcon, San Jose, CA) with RPMI 1640 (Invitrogen) containing 10% FCS (Cansera International), 100 U/ml penicillin, and 100 μg/ml streptomycin (Invitrogen). To propagate podocytes, cells were cultivated at 33°C and treated with 50 U/ml of recombinant mouse IFN-γ (BD Bioscience, Palo Alto, CA) to enhance expression of the large T antigen. After 90% confluence, the cells were induced to differentiate into podocyte lineage by shifting them to 37°C and culturing in DMEM (Sigma) that contained 10% FCS without IFN-γ,

Table 2. *Mean serum insulin, liver weight, heart weight, and right kidney weight in experimental animals*

Group	Week 8			
	Serum Insulin, μg/l	Liver Weight, g	Heart Weight, g	Kidney Weight, g
Nondiabetic	0.30 ± 0.05	1.26 ± 0.05	0.152 ± 0.003	0.202 ± 0.004
Diabetic (vehicle)	2.10 ± 0.50*	2.53 ± 0.08*	0.168 ± 0.006	0.250 ± 0.016*
Diabetic (Ad-LacZ)	2.10 ± 0.41*	2.55 ± 0.29*	0.168 ± 0.009	0.245 ± 0.006*
Diabetic (Ad-VASH-1)	2.00 ± 0.33*	2.55 ± 0.29*	0.150 ± 0.006	0.210 ± 0.009†

Values are means ± SE; n = 6/group. *$P < 0.05$ vs. nondiabetic controls. †$P < 0.05$ vs. diabetic (vehicle) or diabetic (Ad-LacZ).

i.e., nonpermissive conditions. Under this condition, the majority of cells had an arborized shape and expressed podocyte-specific synaptopodin. After 7 days of culture under nonpermissive conditions, the cells were further cultured in DMEM that contained 0.5% FCS for 24 h, and quiescent mature podocytes were incubated with 5.5 mM normal glucose with PBS (NG), NG with 19.5 mM mannitol (NG/Manni), 25 mM high glucose with PBS (HG/V0), HG with 1 nM rhVASH-1 (HG/V1), 10 nM rhVASH-1 (HG/V10), or 20 nM rhVASH-1 (HG/V20) for 24 h. They then were harvested and subjected to Western blot analysis to determine the direct effect of rhVASH-1 on the protein levels of VEGF-A, ZO-1, P-cadherin (R&D Systems, Minneapolis, MN), desmin, FSP-1 (Dako Cytomation), Snail (Abcam), and Slug (Abcam). In other sets of experiments, cells were subjected to immunofluorescent staining for ZO-1 and P-cadherin.

Podocytes were also cultured in the presence of 1, $25(OH)_2D_3$ (10 nM, Chugai Pharmaceutical, Tokyo, Japan) and all-*trans*-retinoic acid (ATRA; 1 μM, Sigma) to induce the expression of nephrin as previously reported (40).

Immunofluorescent studies (cultured podocytes). Mouse podocytes were cultured on eight-well chamber slides precoated with type I collagen (Nunc-Immuno Plate) and then fixed with ice-cold acetone for 5 min. The chamber slides were blocked with Protein Block Serum-Free (Dako Cytomation) and then incubated with primary antibodies, anti-ZO-1, or P-cadherin antibodies for 1 h. Subsequently, the slides were washed three times in PBS and incubated with Alexa Fluor 488-labeled donkey anti-rabbit IgG (A21206; Invitrogen) or Alexa Fluor 546-labeled goat anti-rat IgG (A11081; Invitrogen) for 1 h. After three washes with PBS, Vectashield anti-fade mounting medium (Vector Labs) was applied, the slides were observed by a fluorescence microscope (BZ-Analyzer; Keyence, Osaka, Japan), and images were obtained. Normal rat and hamster IgG were used as negative controls. Cells were double-stained with 4′, 6-diamidino-2-phenylindole HCl to visualize nuclei.

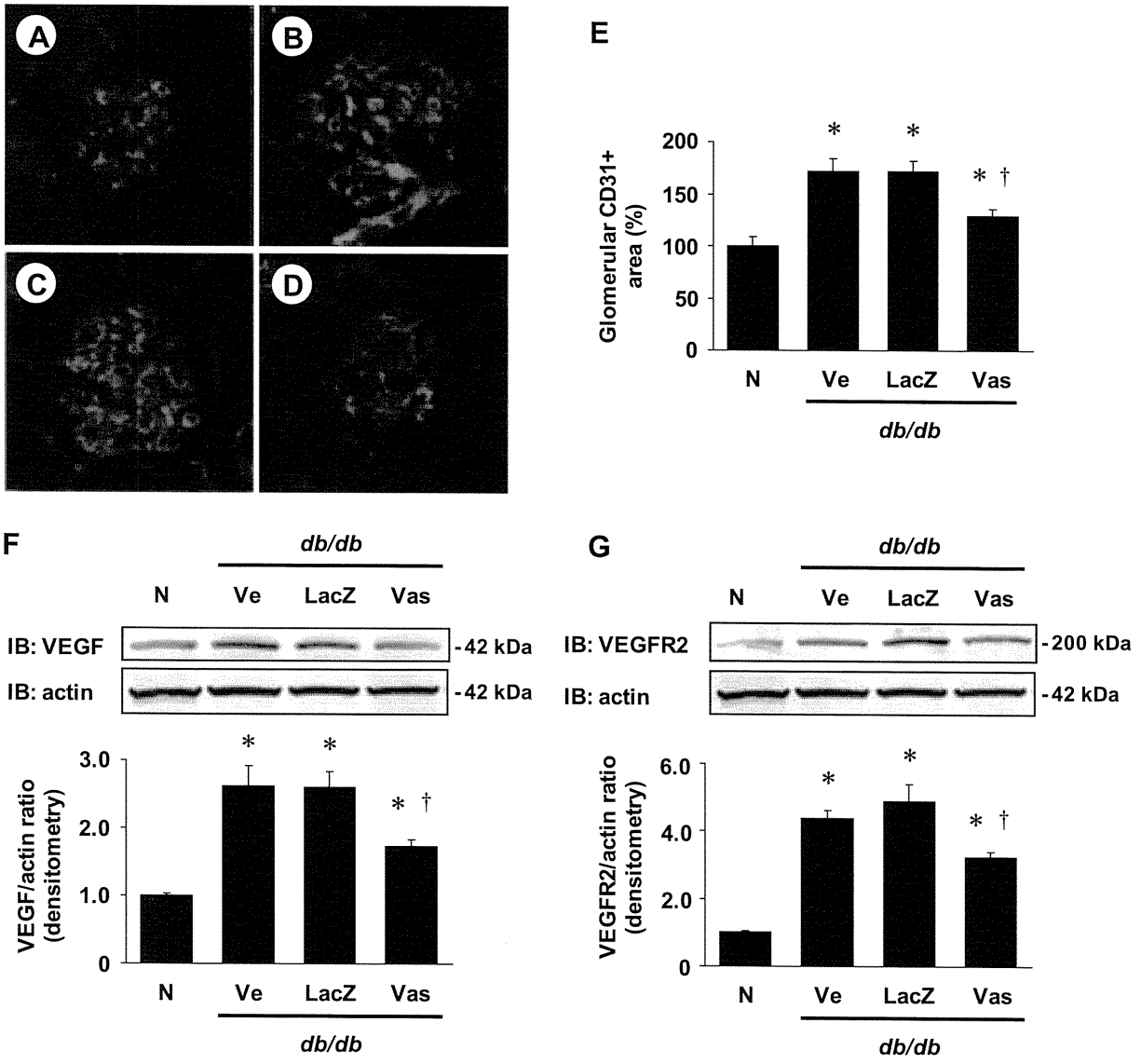

Fig. 2. *A–E*: immunofluorescent staining of CD31, an endothelial cell marker. Distribution of CD31 was determined by indirect immunofluorescence technique in *db/m* mice (*A*), *db/db* mice treated either with vehicle buffer (*B*), AdLacZ (*C*), or AdhVASH-1 (*D*) at 16 wk of age. *E*: glomerular $CD31^+$ endothelial area was quantitated. Increase in the $CD31^+$ glomerular capillary area was significantly suppressed after treatment with AdhVASH-1. $^*P < 0.05$ vs. *db/m*. $\dagger P < 0.05$ vs. Ve or LacZ. *F and G*: immunoblot analysis. Immunoblots for VEGF-A, VEGF receptor (VEGFR)-2, and actin are shown. Each lane was loaded with 50 μg protein obtained from the renal cortex. Each band was scanned and subjected to densitometry. *F*, *bottom*: intensities of VEGF-A protein relative to actin. $^*P < 0.05$ vs. *db/m*. $\dagger P < 0.05$ vs. Ve or LacZ. *G*, *bottom*: intensities of VEGFR-2 protein relative to actin. $^*P < 0.05$ vs. *db/m*. $\dagger P < 0.05$ vs. Ve or LacZ; $n = 6$/group.

RNA extraction and quantitative real-time RT-PCR. Cultured mouse podocytes were homogenized and total RNA was extracted using an RNeasy Midi Kit (Qiagen, Chatsworth, CA) and stored at −80°C until use. Total RNA was subjected to RT using a first-strand cDNA synthesis system (Invitrogen) with random hexamers and reverse transcriptase. Quantitative real-time PCR was used to quantify the mRNA levels of nephrin and the amount of 18S rRNA. cDNA was diluted 1:10 with autoclaved deionized water. For the detection of nephrin mRNA levels, 5 μl of the diluted cDNA was added to the Lightcycler-Mastermix, 0.5 μM of specific primer, 3 mM of $MgCl_2$ and 2 μl of Master SYBR Green. For detecting the level of 18S rRNA, 5 μl of the diluted cDNA was added to the Lightcycler-Mastermix, 0.2 μM of specific primer, 3 mM of $MgCl_2$ and 2 μl of SYBR Premix Ex Taq (Takara Bio). These reaction mixtures were filled to a final volume of 20 μl with water. PCR reactions were carried out in a real-time PCR cycler (Lightcycler; Roche Diagnostics). The program was optimized and performed finally as denaturation at 95°C for 10 min followed by 40 cycles of amplification (nephrin; 95°C for 10 s; 60°C for 10 s; 72°C for 10 s, 18S rRNA; 95°C for 5 s; 60°C for 20 s, respectively). The temperature ramp rate was 20°C/s. At the end of each extension step, the fluorescence was measured to quantitate the PCR products. After completion of the PCR, the melting curve of the product was measured by a temperature gradient from 65 to 95°C at 0.1 or 0.2°C/s with continuous fluorescence monitoring to produce a melting profile of the primers. The amount of PCR products was normalized with 18S rRNA to determine the relative expression ratio for nephrin mRNA. The following oligonucleotide primers specific for mouse nephrin and 18S rRNA were used: nephrin, 5′-ATCTCCAAGACCCCAGGTACACA-3′ (forward) and 5′-AGGGTCAGGACGGCT GAT-3′ (reverse); 18S rRNA, 5′-ACTCAACACGGGAAACCTCA-3′ (forward) and 5′-AACCAGACAAATCGCTCCAC-3′ (reverse). Four independent experiments were performed.

Statistical analysis. All values are expressed as means ± SE. A Kruskal-Wallis test with post hoc comparisons using Fisher's exact test was employed for intergroup comparisons of multiple variables. A level of $P < 0.05$ was considered statistically significant.

RESULTS

Serum and hepatic levels of VASH-1 following adenoviral transfer. The serum and hepatic levels of VASH-1 were detected by immunoblot assay. Serum levels of VASH-1 were at very low levels in both the nondiabetic *db/m* and the control diabetic *db/db* mice (data not shown). The AdhVASH-1-injected diabetic *db/db* mice exhibited significantly elevated serum VASH-1 levels compared with the AdLacZ injection at 2 wk after the final injections (Fig. 1*A*). Similarly, hepatic expression of VASH-1 was markedly elevated in the AdhVASH-1-injected *db/db* mice (Fig. 1*A*). The mice receiving AdLacZ or AdhVASH-1 did not exhibit any deleterious side effects, and all the mice survived. In addition, nondiabetic male *db/m* mice receiving AdhVASH-1 did not exhibit any inflammatory or pathological alterations in the lungs, liver, or kidneys (data not shown), and hypertension or proteinuria was not observed.

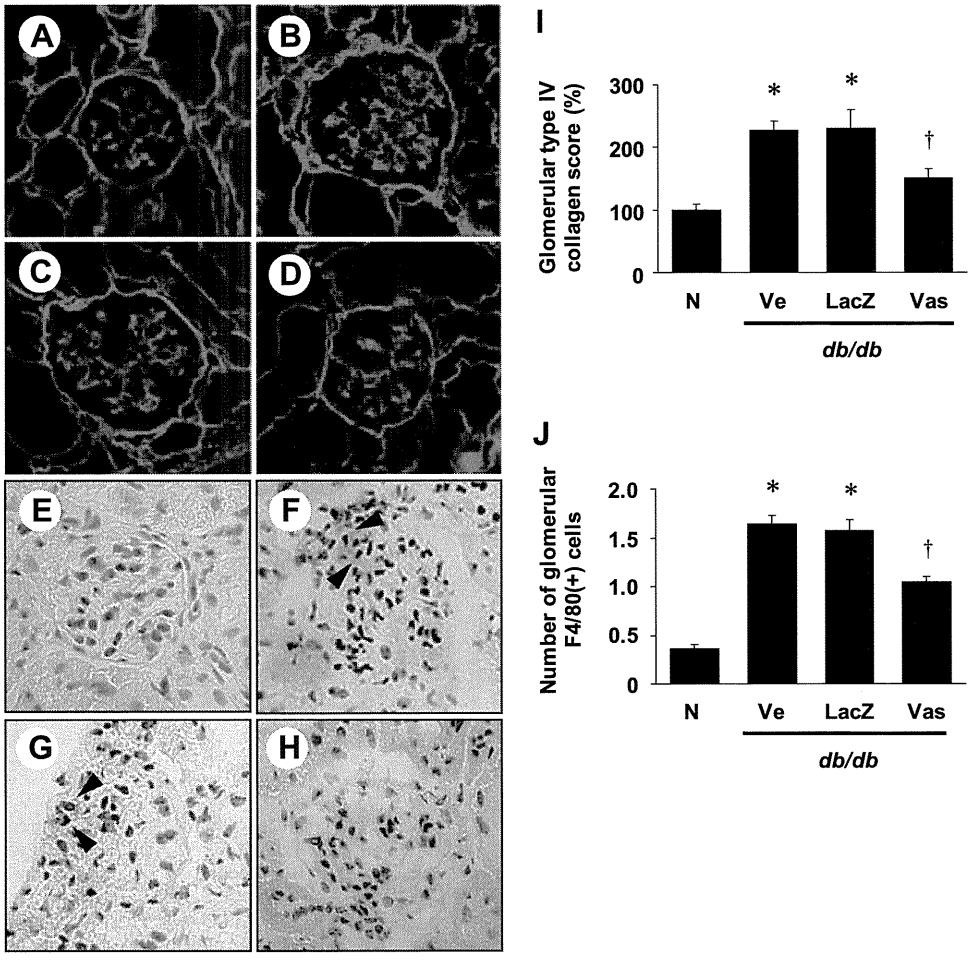

Fig. 3. *A–D*: glomerular accumulation of type IV collagen was assessed by the indirect immunofluorescence method for *db/m* mice (*A*), *db/db* mice treated either with vehicle buffer (*B*), AdLacZ (*C*), or AdhVASH-1 (*D*) at 16 wk of age. Original magnification, ×400. Immunohistochemistry of F4/80$^+$ monocytes/macrophages. Representative light microscopic appearances of glomerulus in *db/m* mice (*E*), *db/db* mice treated with either vehicle buffer (*F*), AdLacZ (*G*), or AdhVASH-1 (*H*) are shown. F4/80$^+$ cells were observed in glomeruli of *db/db* mice (arrowheads; original magnification ×400). *I*: amount of immunoreactive type IV collagen in glomeruli relative to the nondiabetic control *db/m* mice determined by computer image analysis is shown. *J*: number of glomerular F4/80$^+$ monocytes/macrophages is shown. Increase in the number of F4/80$^+$ monocyte/macrophages was significantly suppressed after treatment with AdhVASH-1; n = 6/group. *$P < 0.05$ vs. N. †$P < 0.05$ vs. Ve or LacZ.

Changes in blood glucose, body weight, food consumption, mean serum insulin, liver weight, heart weight, and kidney weight. Body weight, blood glucose, food consumption, serum levels of insulin, liver weight, heart weight, and kidney weight were significantly increased in the *db/db* mice compared with the *db/m* mice at the age of 16 wk. Treatment with AdhVASH-1 did not alter plasma glucose concentrations, food consumption, obesity, and mean serum insulin in *db/db* mice after 8 wk of treatment (Tables 1 and 2). There was no significant difference in liver weight between treatment with AdhVASH-1 and AdLacZ, but the increase in kidney weight in *db/db* mice was significantly suppressed by treatment with AdhVASH-1 compared with AdLacZ (Table 2). Heart weight tended to be lower in the AdhVASH-1-treated group compared with the AdLacZ-treated group without statistical significance (Table 2).

Changes in blood pressure. There were no significant differences in blood pressure measured at the age of 16 wk among the experimental groups (*db/m* mice, 118 ± 5; *db/db* mice treated with vehicle, 114 ± 3; *db/db* mice treated with AdLacZ, 114 ± 3; *db/db* mice treated with AdhVASH-1, 112 ± 5, mmHg).

Changes in serum creatinine, Ccr, and urinary albumin excretion. Serum creatinine levels did not significantly differ among the experimental groups. To evaluate the effect of VASH-1 on preventing hyperfiltration associated with diabetic nephropathy, Ccr and UACR were determined (Fig. 1, *B* and *C*). Although *db/db* mice treated with vehicle or AdLacZ showed a marked elevation of Ccr and UACR, AdhVASH-1 treatment resulted in the suppression of the diabetes-induced increase in Ccr and UACR at 8 wk after initiation of treatment.

Histology and morphometric analysis. Histological examination of the kidneys revealed glomerular hypertrophy and expansion of the mesangial area in vehicle-treated *db/db* mice. At 8 wk after initiation of treatment with AdhVASH-1, glomerular hypertrophy and mesangial matrix expansion were significantly inhibited compared with the control diabetic animals (Fig. 1, *D–G*). Morphometric analysis (Fig. 1, *H* and *I*) further confirmed the inhibitory effects of AdhVASH-1 on these parameters.

Immunohistochemical analysis of $CD31^+$ endothelial area. We next evaluated differences in the $CD31^+$ glomerular endothelial area by immunofluorescence staining. In *db/m* mice, immunoreactivity for CD31 was detected in glomerular capillaries (Fig. 2*A*), and an increase in the $CD31^+$ area in glomeruli was observed in the control diabetic *db/db* mice (Fig. 2, *B* and *C*). Treatment with AdhVASH-1 significantly suppressed the increase in the glomerular $CD31^+$ area compared with AdLacZ (Fig. 2*D*), confirmed by quantitative analysis (Fig. 2*E*). We also evaluated the $CD31^+$ PTC endothelial area to determine the potential adverse effects of VASH-1 on the survival of PTC at 8 wk after initiating treatment. No significant difference of PTC density was observed among experimental groups (Supplementary Fig. S1; all supplementary material for this article is available on the journal web site).

Protein levels of VEGF-A and receptor VEGFR-2 in the renal cortex. The effect of AdhVASH-1 on the expression of proangiogenic factor VEGF-A and corresponding receptors VEGFR-2 in the renal cortex was studied by immunoblot assay. The level of VEGF-A and VEGFR-2 was significantly increased in *db/db* mice, which is consistent with the findings of previous reports (7, 17, 18, 29), and treatment with AdhVASH-1 significantly suppressed the increase in VEGF-A and VEGFR-2 compared with AdLacZ in *db/db* mice (Fig. 2, *F* and *G*).

Immunohistochemical analysis of glomerular type IV collagen. Next, the accumulation of glomerular type IV collagen was examined by immunofluorescence staining (Fig. 3). The amount of type IV collagen in glomeruli was increased in the control *db/db* mice (Fig. 3, *B* and *C*) compared with nondiabetic *db/m* mice (Fig. 3*A*). Enhanced immunoreactivity in the diabetic mice was observed mainly in the glomerular basement membrane and mesangial area. Treatment with AdhVASH-1 decreased the accumulation of type IV collagen compared with AdLacZ treatment in *db/db* mice (Fig. 3*D*), and these results were further confirmed by quantitative morphometric analysis (Fig. 3*I*).

Immunohistochemical analysis of monocyte/macrophage accumulation. We next examined the glomerular infiltration of monocytes/macrophages by immunohistochemistry for F4/80.

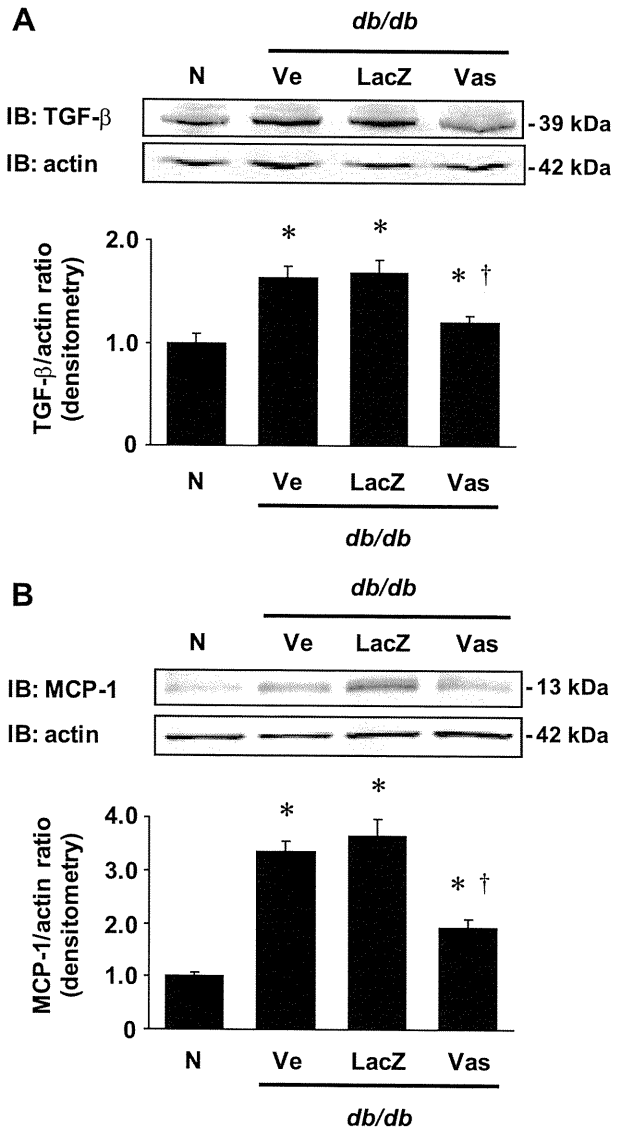

Fig. 4. Immunoblot analysis of transforming growth factor (TGF)-β and monocyte chemoattractant protein-1 (MCP-1). *A* and *B*: immunoblots for TGF-β, MCP-1, and actin. Each lane was loaded with 50 μg protein obtained from the renal cortex. *A*, *bottom*: intensities of TGF-β protein relative to actin. *B*, *bottom*: intensities of MCP-1 protein relative to actin. *$P < 0.05$ vs. *db/m*. †$P < 0.05$ vs. Ve or LacZ; $n = 6$/group.

In the vehicle-treated *db/db* mice (Fig. 3*F*), the number of F4/80$^+$ cells in glomeruli was significantly increased compared with the nondiabetic *db/m* mice (Fig. 3*E*). Treatment with AdhVASH-1 markedly decreased the glomerular accumulation of monocytes/macrophages compared with AdLacZ treatment (Fig. 3, *G*, *H*, and *J*).

Protein levels of TGF-β1 and MCP-1 in the renal cortex. TGF-β1 plays crucial roles in mesangial matrix expansion and renal hypertrophy in diabetic nephropathy (35). MCP-1 is a crucial chemokine involved in the development of diabetic nephropathy (42). The control diabetic *db/db* mice exhibited increased protein levels of TGF-β and MCP-1 compared with

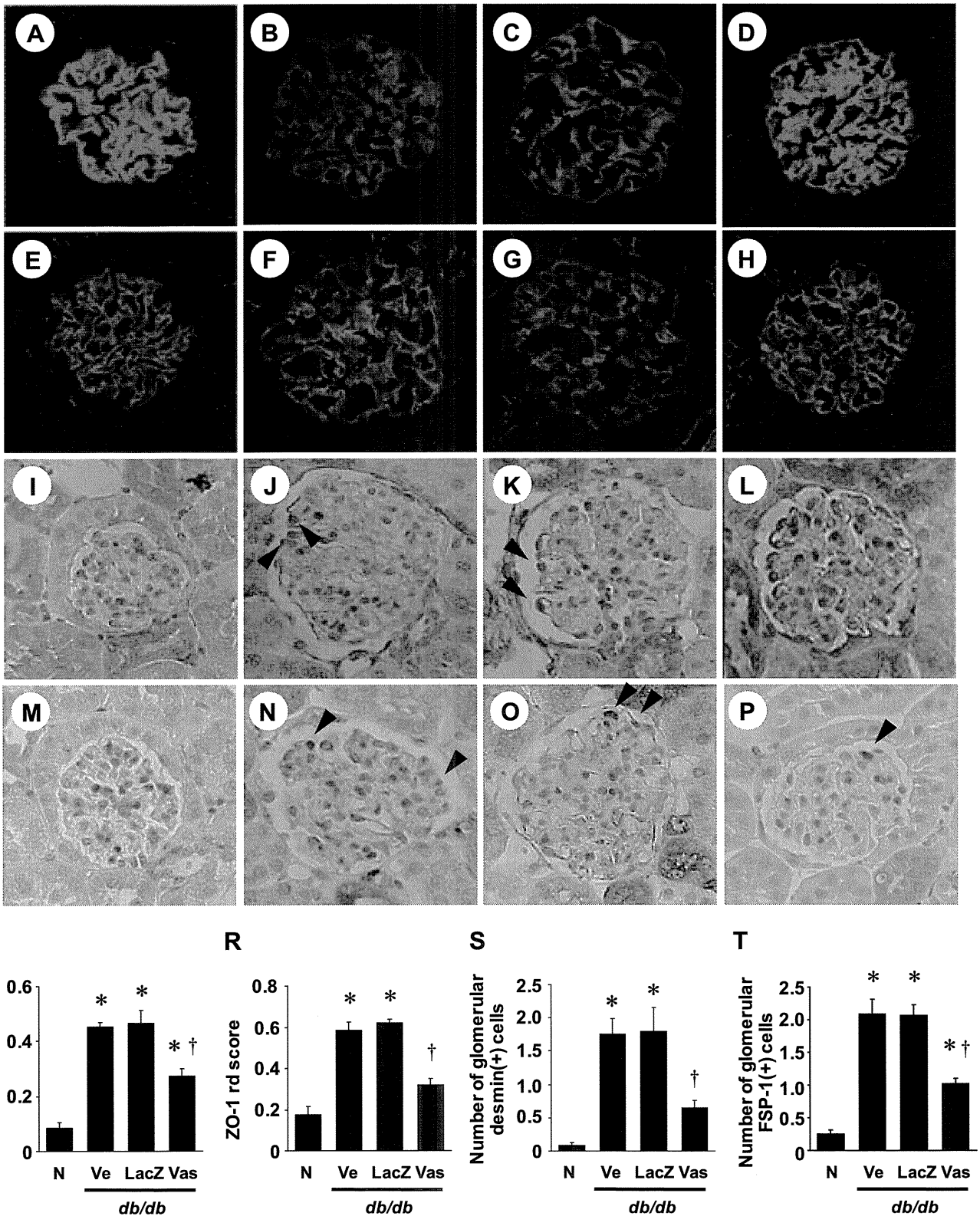

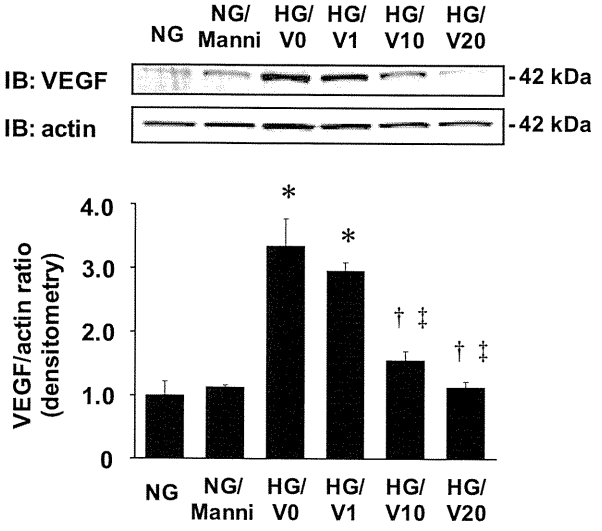

Fig. 6. Immunoblot analysis (cultured podocytes). Immunoblots for VEGF-A and actin are shown. Cells were cultured under normal glucose (NG; 5.5 mM) or high glucose (HG; 25 nM) for 24 h in the presence of recombinant VASH-1 (0–20 nM). In each lane, 20 μg protein obtained from cultured mouse podocytes was loaded. *Bottom*: intensities of VEGF-A protein relative to actin. NG+Manni, normal D-glucose plus D-mannitol (19.5 mmol/L); V0, without VASH-1; V1, 1 nM VASH-1; V10, 10 nM VASH-1; V20, 20 nM VASH-1. *$P < 0.01$ vs. NG or NG/Manni. †$P < 0.05$ vs. HG/V0. ‡$P < 0.01$ vs. HG/V1; $n = 6$/group.

the nondiabetic *db/m* mice in the renal cortex, as detected by immunoblotting. AdhVASH-1 significantly suppressed the increase in TGF-β and MCP-1 compared with AdLacZ in the diabetic animals (Fig. 4, *A* and *B*).

Immunohistochemical analysis of podocyte injuries and slit diaphragm proteins. Since we observed antialbuminuric effects of VASH-1, we next evaluated the degree of podocyte injuries among the experimental groups by immunohistochemistry for nephrin, ZO-1, desmin, and FSP-1. In the nondiabetic *db/m* mice, localization of nephrin (Fig. 5*A*) and ZO-1 (Fig. 5*E*) was observed along the glomerular capillary wall in a continuous pattern, suggesting the localization in podocytes. In contrast, immunoreactivity for desmin, a marker for mesenchymal phenotype and podocyte injuries, was not observed in the nondiabetic *db/m* mice (Fig. 5*I*). Similarly, immunoreactivity for FSP-1, a marker of EMT, was not observed in the glomeruli in nondiabetic *db/m* mice (Fig. 5*M*). In the control diabetic *db/db* mice, the intensity of nephrin and ZO-1 staining was diminished and observed as a discontinuous pattern along the glomerular capillary walls (Fig. 5, *B*, *C*, *F*, and *G*), and immunoreactivity for desmin and FSP-1 was observed along the periphery of glomerular capillaries (Fig. 5, *J*, *K*, *N*, and *O*), suggesting podocyte injuries. Treatment with AdhVASH-1 restored the protein levels as well as the continuous patterns for nephrin and ZO-1 and suppressed the number of desmin$^+$ and FSP-1$^+$ cells in *db/db* mice (Fig. 5, *D*, *H*, *L*, and *P*).

Protein levels of VEGF-A in cultured mouse podocytes. We next performed cell culture analysis using mouse podocytes to examine the potential direct effects of VASH-1 on podocytes in association with its antialbuminuric effects. The protein level of VEGF-A in podocytes was significantly increased at 24 h under the HG condition compared with the NG condition as detected by immunoblotting (Fig. 6). Addition of mannitol to the NG condition did not lead to the increase in VEGF-A, thus excluding the potential effect by elevated osmotic pressure. Treatment with rhVASH-1 resulted in the suppression of the increase in VEGF-A protein induced by HG in a dose-dependent manner (Fig. 6).

Protein levels of ZO-1, P-cadherin, desmin, and FSP-1 in cultured mouse podocytes. The effects of rhVASH-1 on the expression of ZO-1 and P-cadherin (epithelial cell proteins) or desmin and FSP-1 (mesenchymal cell markers) in podocytes were studied by immunoblotting. The levels of P-cadherin and ZO-1 in podocytes were significantly decreased at 24 h under HG compared with NG. In contrast, the protein levels of desmin and FSP-1 were significantly increased at 24 h under HG. Treatment with rhVASH-1 significantly recovered the HG-induced loss of P-cadherin and ZO-1 protein (Fig. 7, *A–C*) and suppressed the HG-induced increase in protein levels of desmin and FSP-1 (Fig. 7, *D–F*).

Protein levels of Snail and Slug in cultured mouse podocytes. We next examined the expression of Snail and Slug, the transcription factors involved in EMT, in podocytes. The protein levels of Snail and Slug were increased at 24 h after incubating under HG compared with NG as detected by immunoblotting. Treatment with rhVASH-1 significantly suppressed the increase in the protein levels of Snail and Slug induced by HG (Fig. 8, *A* and *B*).

Immunohistochemical analysis of ZO-1 and P-cadherin in cultured mouse podocytes. Immunofluorescence staining showed that ZO-1 and P-cadherin were localized in the cell-to-cell junctions of podocytes under NG, and immunoreactivity for these proteins was diminished under HG. Treatment with rhVASH-1 markedly recovered the immunoreactivity for ZO-1 and P-cadherin in the cell-to-cell junctions of podocytes (Fig. 9).

mRNA levels of nephrin in cultured mouse podocytes. Since the expression of nephrin is hardly detectable in these cultured mouse podocytes, we induced the expression of nephrin in the presence of 1, 25$(OH)_2D_3$ and all-*trans*-retinoic acid (VRAD)

Fig. 5. *A–D*: immunofluorescent staining of nephrin. Distribution of nephrin was determined by indirect immunofluorescence technique in *db/m* mice (*A*), *db/db* mice treated either with vehicle buffer (*B*), AdLacZ (*C*), or AdhVASH-1 (*D*) at 16 wk of age. *E–H:* immunofluorescent staining of ZO-1. Distribution of ZO-1 was determined by indirect immunofluorescence technique in *db/m* mice (*E*), *db/db* mice treated either with vehicle buffer (*F*), AdLacZ (*G*), or AdhVASH-1 (*H*) at 16 wk of age. *I–L*: immunohistochemistry of desmin$^+$ podocytes. Representative light microscopic appearance of glomeruli for *db/m* mice (*I*), *db/db* mice treated with either vehicle buffer (*J*), AdLacZ (*K*), or AdhVASH-1 (*L*) at 16 wk of age is shown. Desmin$^+$ podocytes (arrowheads) were frequently observed in *db/db* mice treated with either vehicle buffer (*J*) or AdLacZ (*K*). *M–P*: immunohistochemistry of fibroblast-specific protein-1 (FSP-1$^+$) podocytes. Representative light microscopic appearance of glomeruli for *db/m* mice (M), *db/db* mice treated with either vehicle buffer (N), AdLacZ (O), or AdhVASH-1 (P) at 16 wk of age is shown. FSP-1$^+$ podocytes (arrowheads) were frequently observed in *db/db* mice treated with either vehicle buffer (*J*) or AdLacZ (*K*). *Q* and *R*: staining score for nephrin and ZO-1 are shown as "redistribution (rd) score." The staining patterns of nephrin and ZO-1 were evaluated using the method described in MATERIALS AND METHODS. *S* and *T*: number of desmin$^+$ or FSP-1$^+$ podocytes. Increase in the number of desmin$^+$ or FSP-1$^+$ podocytes in the diabetic animals was significantly suppressed by treatment with AdhVASH-1. *Q–T*: $n = 6$/group. Original magnification ×400. *$P < 0.05$ vs. *db/m*. †$P < 0.05$ vs. Ve or LacZ.

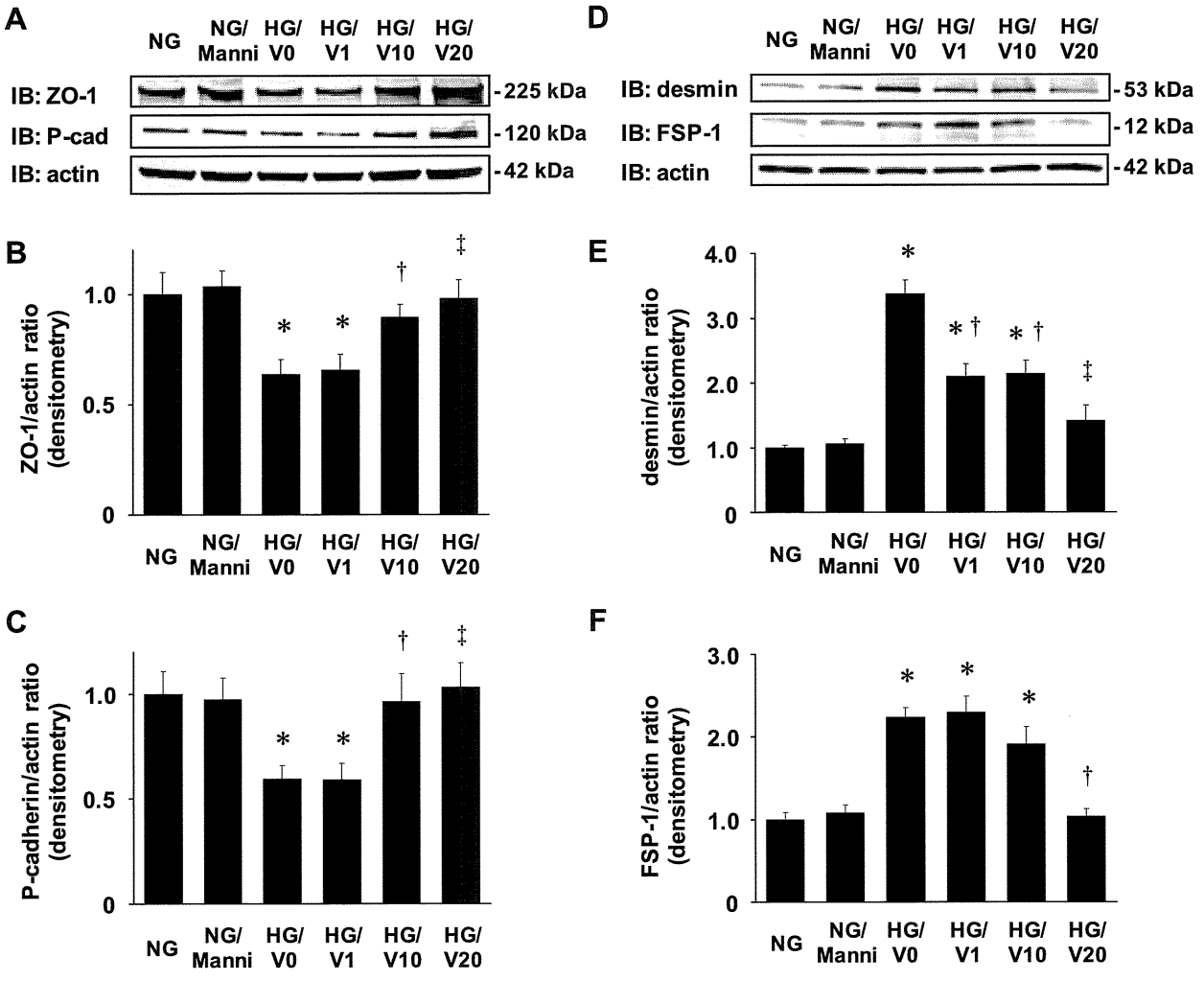

Fig. 7. *A–F*: immunoblot analysis (cultured podocytes). *A* and *D*: immunoblots for ZO-1, P-cadherin (P-cad), desmin, FSP-1, and actin. Each lane was loaded with 20 μg protein obtained from cultured mouse podocytes. *B*: intensities of ZO-1 protein relative to actin. *$P < 0.01$ vs. NG or NG/Manni. †$P < 0.05$ vs. HG/V0 or HG/V1. ‡$P < 0.01$ vs. HG/V0 or HG/V1. *C*: intensities of P-cadherin protein relative to actin. *$P < 0.01$ vs. NG or NG/Manni. †$P < 0.05$ vs. HG/V0 or HG/V1. ‡$P < 0.01$ vs. HG/V0 or HG/V1. *E*: intensities of desmin protein relative to actin. *$P < 0.01$ vs. NG or NG/Manni. †$P < 0.01$ vs. HG/V0. ‡$P < 0.01$ vs. HG/V0, HG/V1 or HG/V10. *F*: intensities of FSP-1 protein relative to actin. *$P < 0.01$ vs. NG or NG/Manni. †$P < 0.01$ vs. HG/V0, HG/V1 or HG/V10.

as previously described (40). Sufficient induction of nephrin mRNA was confirmed as detected by real-time PCR in podocytes under VRAD and NG, but nephrin mRNA levels were significantly reduced under VRAD and HG (Fig. 10). Treatment with rhVASH-1 significantly recovered the HG-induced loss of nephrin mRNA (Fig. 10).

Levels of endogenous mouse VASH-1 in nondiabetic and diabetic mouse kidneys. We next examined the levels of endogenous mouse VASH-1 protein levels in the kidneys of the experimental groups as detected by Western blotting. Renal levels of mouse VASH-1 were increased in the control diabetic mice compared with nondiabetic mice. Treatment with AdhVASH-1 did not affect endogenous VASH-1 levels in diabetic mice (Fig. 11).

DISCUSSION

In the present study, we utilized *db/db* mice to demonstrate the therapeutic efficacy of VASH-1 on renal alterations. The *db/db* mouse is characterized by obesity, sustained hyperglycemia, hyperinsulinemia and lack of ketonuria, due to the defect of the leptin receptor in the hypothalamus, exhibiting the typical diabetic renal alterations characterized within 2 mo of diabetes.

Renal levels of endogenous mouse VASH-1 were increased in the control diabetic mice compared with nondiabetic mice, suggesting the compensatory increase in VASH-1 in response to an excessive angiogenic milieu with elevation of VEGF-A. Treatment with AdhVASH-1 did not alter the levels of endogenous mouse VASH-1 in kidney. Based on these findings, we speculate that the increase in mouse VASH-1 in the diabetic kidney may not be sufficient to counteract the effects of angiogenic stimuli such as VEGF-A, requiring the supplementation of exogenous VASH-1 to effectively suppress the progression of diabetic nephropathy.

Intravenous administration of AdhVASH-1 resulted in the sustained increase in serum levels of hVASH-1 presumably derived from the liver, without causing any systemic inflammation. Additionally, administration of AdhVASH-1 in nondiabetic mice did not cause any renal inflammatory alterations (data not shown). Therefore, we consider the present approach

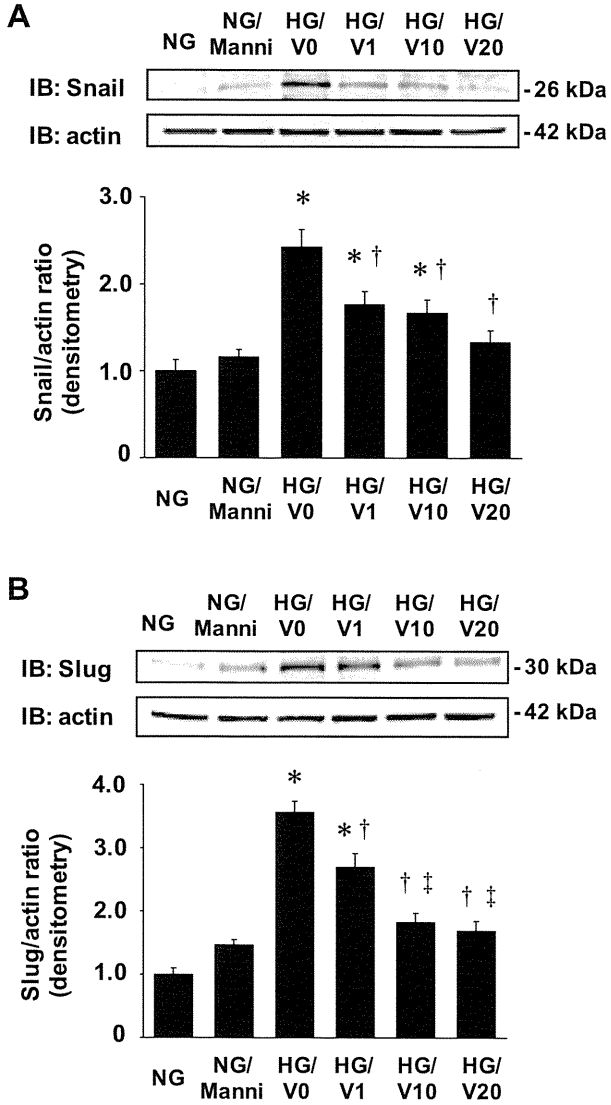

Fig. 8. *A* and *B*: immunoblot analysis (cultured podocytes). *A* and *B*: immunoblots for Snail, Slug, and actin. Each lane was loaded with 20 μg protein obtained from cultured mouse podocytes. *A*, *bottom*: intensities of Snail protein relative to actin. *$P < 0.01$ vs. NG or NG/Manni. †$P < 0.05$ vs. HG/V0. ‡$P < 0.005$ vs. HG/V1; $n = 6$/group. *B*, *bottom*: intensities of Slug protein relative to actin. *$P < 0.01$ vs. NG or NG/Manni. †$P < 0.01$ vs. HG/V0. ‡$P < 0.01$ vs. HG/V1 or HG/V10; $n = 6$/group.

employing adenoviral vectors to be nonharmful for experimental animals. AdhVASH-1 treatment did not affect blood glucose, body weight, food consumption, or serum insulin concentration in *db/db* mice. Previous reports have described inconsistent results on Ccr within 2 mo of the onset of diabetes in *db/db* mice (6, 12). The discrepant outcomes may be attributed to a variable susceptibility to diabetes in subbreedings of the *db/db* mouse strain. In the present study, we observed increased Ccr and albuminuria in vehicle-treated *db/db* mice. In addition, characteristic histological alterations in diabetic nephropathy such as glomerular hypertrophy and the increase in mesangial matrix were observed in the control diabetic mice. These abnormalities in diabetic nephropathy were significantly inhibited by AdhVASH-1 compared with AdLacZ treatment at 8 wk after initiation of treatment. The suppressive effects of AdhVASH-1 on albuminuria were rather modest compared with the suppressive effects on the increase in Ccr, suggesting the requirement of additional factors or the involvement of distinct mechanisms in albuminuria in diabetic nephropathy.

Experimental type 1 and type 2 diabetes animals exhibit an increased glomerular filtration surface area, glomerular capillary length, and/or glomerular capillary number (14, 30). Treatment with AdhVASH-1 suppressed the increase in the $CD31^+$ glomerular endothelial area in *db/db* mice, potentially via its antiangiogenic efficacy, thus leading to the observed suppressive effects on the increase in Ccr and albuminuria.

Previous studies demonstrated the therapeutic effects of neutralizing anti-VEGF-A antibodies in diabetic nephropathy models (8, 12) and amelioration of diabetic nephropathy in mice with inducible overexpression of sFlt-1 in podocytes (21). In the present study, we observed increased renal levels of VEGF-A in the diabetic control mice, consistent with the findings of previous reports (7, 29, 41, 48). On the contrary, recent reports have demonstrated reduced expression of VEGF-A in human diabetic nephropathy (1, 23). Although diabetic animal models are often studied in a relatively early phase of the disease, most diabetic patients employed in clinical studies were already in a moderately advanced stage. In a study using samples of human diabetic nephropathy, reduced interstitial VEGF-A expression was associated with interstitial vascular rarefaction (23), but we detected no reduction of PTC density in the present study in the control *db/db* mice. Treatment with AdhVASH-1 suppressed the increase in VEGF-A as well as flk-1 in the renal cortex. In our previous analysis, AdhVASH-1 treatment failed to suppress renal levels of VEGF-A, but suppressed the levels of flk-1 in type 1 diabetic mice (29). The discrepant results regarding the regulation of renal VEGF-A levels by VASH-1 between type 1 and 2 diabetes models may be attributed to the difference in models of diabetes and stages of diabetic nephropathy. Since podocytes are the main source of VEGF-A in glomeruli, we then examined the potential direct effect of VASH-1 on the synthesis of VEGF-A induced by high glucose in podocytes. We observed the inhibitory effect of VASH-1 on high glucose-induced upregulation of VEGF-A in cultured mouse podocytes.

Renal hypertrophy observed in the control *db/db* mice was significantly suppressed by AdhVASH-1. VEGF-A augments protein synthesis and hypertrophy in renal proximal tubular epithelial cells (34). Considering the dominant contribution of the tubular compartment in organizing renal mass, VASH-1 might have regulated glomerular as well as tubular hypertrophy potentially via regulating VEGF-A-mediated signaling.

The accumulation of type IV collagen in glomeruli in *db/db* mice was also inhibited by AdhVASH-1, potentially associated with the suppression of renal TGF-β1 levels. These results are consistent with the inhibitory effects of other antiangiogenic reagents on ECM accumulation in animal models of diabetic nephropathy (17, 18, 44, 48, 50). We recently reported the inhibitory effects of recombinant VASH-1 on the high glucose-induced increase in TGF-β in cultured mesangial cells (29), suggesting the possibility of the direct effects of VASH-1 on mesangial cells leading to ameliorated accumulation of glomerular type IV collagen. In addition, podocyte-derived VEGF-A induced by TGF-β1 was reported to stimulate the production of α_3(IV) collagen, a component of α-chains in GBM (5). Therefore,

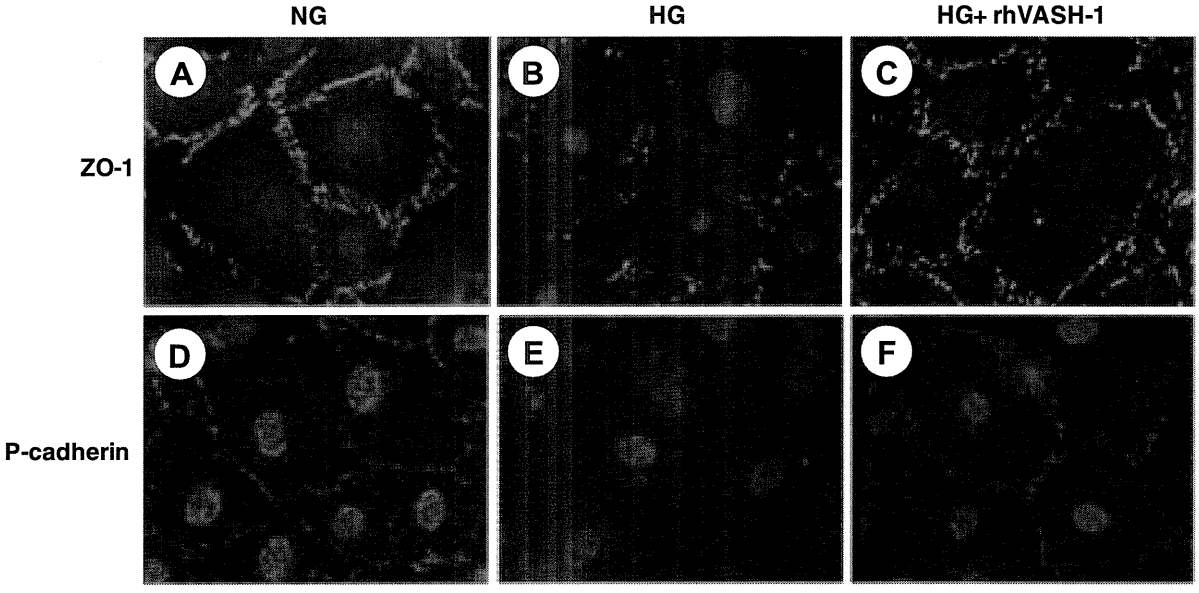

Fig. 9. *A–C*: immunofluorescent staining of zonula occludens (ZO)-1. Distribution of ZO-1 (green) was determined by indirect immunofluorescence technique in cultured podocytes incubated with NG (*A*), HG without rhVASH-1(*B*), or HG with 20 nM rhVASH-1 (*C*). *D–F*: immunofluorescent staining of P-cadherin. Distribution of P-cadherin (red) was determined by indirect immunofluorescence staining in cultured podocytes incubated with NG (*D*), HG without rhVASH-1 (*E*), or HG with 20 nM rhVASH-1 (*F*). Cells were double stained with 4′,6-diamino-2-phenylindole HCL to visualize the nuclei. Original magnification ×400.

the inhibitory effect of VASH-1 on mesangial matrix expansion may also be mediated through regulation of VEGF-A, which presumably is involved in mediating the profibrotic effect of TGF-β1 in diabetic nephropathy.

The potential role of VEGF-A in mediating glomerular monocyte/macrophage infiltration has been demonstrated in a diabetic animal model (33). The anti-inflammatory effect of VASH-1 observed in the present study might be associated with regulation of vascular permeability through suppressing overactivation of VEGF-A signaling and with inhibition of renal MCP-1 levels. In fact, the therapeutic effect of VASH-1 on the formation of arterial neointima in association with inhibitory effects on adventitial macrophage infiltration has been reported (49). Since infiltration of macrophages and mesangial accumulation of ECM proteins are associated in diabetic nephropathy (31, 32), the observed anti-inflammatory effects of VASH-1 might have contributed to the inhibition of mesangial matrix accumulation.

Podocyte injury in association with altered expression of slit diaphragm proteins is involved in proteinuria in diabetic nephropathy. In addition, recent reports suggested the involvement of EMT-like alterations in podocytes in association with the loss of glomerular filtration barrier function in diabetic nephropathy (22, 47). Since AdhVASH-1 showed inhibitory effects on albuminuria in *db/db* mice, we evaluated the expression of nephrin, ZO-1, and P-cadherin, important components of the slit diaphragm cell adhesion complexes (3). We ob-

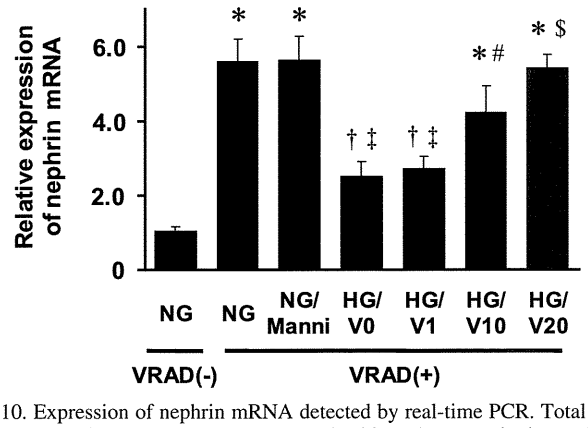

Fig. 10. Expression of nephrin mRNA detected by real-time PCR. Total RNA was extracted from cultured podocytes and subjected to quantitative real-time PCR as described in MATERIALS AND METHODS. The amount of nephrin mRNA relative to 18S rRNA is shown. Results were expressed relative to NG-VRAD(−) that were arbitrarily assigned a value of 1.0. *$P < 0.01$ vs. NG-VRAD(−). †$P < 0.05$ vs. NG-VRAD(−). ‡$P < 0.01$ vs. NG-VRAD(+) or NG/Manni-VRAD(+). #$P < 0.05$ vs. HG/V0-VRAD(+) or HG/V1-VRAD(+). \$$P < 0.01$ vs. HG/V0-VRAD(+) or HG/V1-VRAD(+); $n = 6$/group.

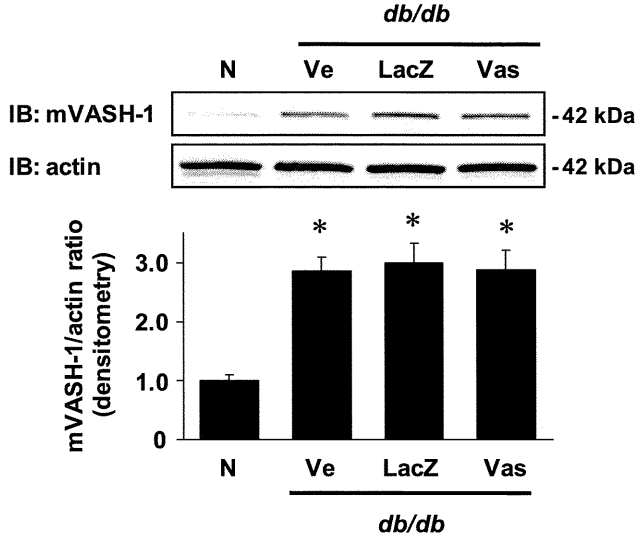

Fig. 11. Immunoblot analysis of mVASH-1. Immunoblots for mVASH-1 and actin are shown. Each lane was loaded with 50 μg protein obtained from the renal cortex. *Bottom*: intensities of mVASH-1 protein relative to actin. *$P <$ 0.05 vs. *db/m*; $n = 6$/group.

served the reduction as well as altered localization of nephrin, P-cadherin, and ZO-1 in the control *db/db* mice, and AdhVASH-1 treatment significantly recovered the altered expression of these proteins. The inhibitory effects of AdhVASH-1 on the increase in desmin$^+$ podocytes and FSP-1$^+$ podocytes further confirmed the protective effects of VASH-1 on podocytes via suppressing EMT-like alterations. VASH-1 further maintained the levels of nephrin, epithelial cell-specific proteins (ZO-1 and P-cadherin) and reduced the levels of mesenchymal proteins (desmin and FSP-1) under HG in cultured podocytes. In addition, the HG-induced increase in the protein levels of transcription factors Snail and Slug, involved in the induction of EMT, was inhibited by VASH-1. Our results suggest the potential therapeutic effects of VASH-1 via counteracting EMT-like alterations and maintaining the characteristic phenotype of podocytes in diabetic nephropathy.

There are several limitations to the present study. In the advanced stage of diabetes, antiangiogenic reagents may impair neovessel formation, leading to deterioration of macrovascular complications such as myocardial infarction and limb ischemia. However, AdhVASH-1 might be tolerable or even therapeutic for atherosclerotic conditions considering the therapeutic effects of AdhVASH-1 in preventing neointimal formation (49). The crucial involvement of chronic hypoxia in association with a reduction of PTC in progressing tubulointerstitial injuries has been reported (28). AdhVASH-1 did not reduce PTC density in the present model, suggesting its safety in diabetic nephropathy. However, careful evaluation on the potential influence of VASH-1 on PTC density at a more advanced stage of diabetic nephropathy might be required.

Recently, the potential adverse events of bevacizumab, a humanized monoclonal antibody against VEGF-A, resulting in thrombotic microangiopathy have been reported in patients with cancer (10). The lack of such histological alterations in previous experimental diabetic nephropathy models employing anti-VEGF-A antibodies or SU5416 (8, 12, 38) as well as amelioration of diabetic glomerular alterations by inducible podocyte-specific overexpression of sFlt-1 in adult mice (21) suggest that anti-VEGF-A therapy might not be detrimental for patients with diabetic nephropathy. In fact, systemic delivery of sFlt-1 resulted in the protection of podocytes associated with reduction of albuminuria, but led to the exacerbation of tubulointerstitial injuries accompanied by peritubular capillary loss in *db/db* mice (20). Although VASH-1 suppresses overactivation of VEGFR-2 (29), it does not serve as a specific inhibitor of VEGF signaling (45), does not cause apoptosis of normal vascular endothelial cells (16), and did not cause peritubular capillary loss or tubulointerstitial injuries in the present study. In addition, AdhVASH-1 did not cause proteinuria in nondiabetic mice. Thus VASH-1 treatment is distinct from strategies with specific inhibition of VEGF-A, potentially associated with fewer adverse events. The identification of specific receptors for VASH-1 is underway. Alteration in the expression of VASH-1 in the normal kidney and in patients with renal disorders is also under investigation.

In conclusion, we demonstrated that VASH-1 effectively ameliorates renal alterations in an animal model of type 2 diabetes. Our results implicate the direct effects of VASH-1 on glomerular podocytes for the first time in association with anti-proteinuric mechanisms via maintaining the epithelial phenotype. We believe that our present study will eventually guide us to the development of novel therapeutic strategies for patients with diabetic nephropathy.

ACKNOWLEDGMENTS

We are grateful to Prof. Toshiyoshi Fujiwara (Center for Gene and Cell Therapy, Okayama Univ. Hospital) for technical assistance in preparing adenoviral vectors.

A portion of this work was published in abstract form (*J Am Soc Nephrol* 18: 654A, 2007).

GRANTS

A portion of this study was supported by a research grant from a Grant-in-Aid for Scientific Research from the Ministry of Education, Science and Culture of Japan (2005–2010, Y. Maeshima), a Grant-in-Aid from the Japan Diabetes Foundation (2005, Y. Maeshima), the Takeda Science Foundation (2006–2010, Y. Maeshima), and the Japan Foundation of Cardiovascular Research (2006, Y. Maeshima). Part of this work was carried out under the Cooperative Research Project Program of the Institute of Development, Aging, and Cancer, Tohoku University.

DISCLOSURES

No conflicts of interest, financial or otherwise, are declared by the authors.

REFERENCES

1. **Baelde HJ, Eikmans M, Lappin DW, Doran PP, Hohenadel D, Brinkkoetter PT, van der Woude FJ, Waldherr R, Rabelink TJ, de Heer E, Bruijn JA.** Reduction of VEGF-A and CTGF expression in diabetic nephropathy is associated with podocyte loss. *Kidney Int* 71: 637–645, 2007.
2. **Benigni A, Gagliardini E, Tomasoni S, Abbate M, Ruggenenti P, Kalluri R, Remuzzi G.** Selective impairment of gene expression and assembly of nephrin in human diabetic nephropathy. *Kidney Int* 65: 2193–2200, 2004.
3. **Benzing T.** Signaling at the slit diaphragm. *J Am Soc Nephrol* 15: 1382–1391, 2004.
4. **Brownlee M, Cerami A, Vlassara H.** Advanced glycosylation end products in tissue and the biochemical basis of diabetic complications. *N Engl J Med* 318: 1315–1321, 1988.
5. **Chen S, Lee JS, Iglesias-de la Cruz MC, Wang A, Izquierdo-Lahuerta A, Gandhi NK, Danesh FR, Wolf G, Ziyadeh FN.** Angiotensin II stimulates alpha3(IV) collagen production in mouse podocytes via TGF-beta and VEGF signalling: implications for diabetic glomerulopathy. *Nephrol Dial Transplant* 20: 1320–1328, 2005.
6. **Cohen MP, Clements RS, Cohen JA, Shearman CW.** Prevention of decline in renal function in the diabetic db/db mouse. *Diabetologia* 39: 270–274, 1996.
7. **Cooper ME, Vranes D, Youssef S, Stacker SA, Cox AJ, Rizkalla B, Casley DJ, Bach LA, Kelly DJ, Gilbert RE.** Increased renal expression of vascular endothelial growth factor (VEGF) and its receptor VEGFR-2 in experimental diabetes. *Diabetes* 48: 2229–2239, 1999.
8. **de Vriese AS, Tilton RG, Elger M, Stephan CC, Kriz W, Lameire NH.** Antibodies against vascular endothelial growth factor improve early renal dysfunction in experimental diabetes. *J Am Soc Nephrol* 12: 993–1000, 2001.
9. **Dvorak HF, Brown LF, Detmar M, Dvorak AM.** Vascular permeability factor/vascular endothelial growth factor, microvascular hyperpermeability, and angiogenesis. *Am J Pathol* 146: 1029–1039, 1995.
10. **Eremina V, Jefferson JA, Kowalewska J, Hochster H, Haas M, Weisstuch J, Richardson C, Kopp JB, Kabir MG, Backx PH, Gerber HP, Ferrara N, Barisoni L, Alpers CE, Quaggin SE.** VEGF inhibition and renal thrombotic microangiopathy. *N Engl J Med* 358: 1129–1136, 2008.
11. **Ferrara N.** Vascular endothelial growth factor and the regulation of angiogenesis. *Recent Prog Horm Res* 55: 15–35, 2000.
12. **Flyvbjerg A, Dagnaes-Hansen F, De Vriese AS, Schrijvers BF, Tilton RG, Rasch R.** Amelioration of long-term renal changes in obese type 2 diabetic mice by a neutralizing vascular endothelial growth factor antibody. *Diabetes* 51: 3090–3094, 2002.
13. **Folkman J.** Angiogenesis in cancer, vascular, rheumatoid and other disease. *Nat Med* 1: 27–31, 1995.

14. **Guo M, Ricardo SD, Deane JA, Shi M, Cullen-McEwen L, Bertram JF.** A stereological study of the renal glomerular vasculature in the db/db mouse model of diabetic nephropathy. *J Anat* 207: 813–821, 2005.
15. **Hashimoto N, Maeshima Y, Satoh M, Odawara M, Sugiyama H, Kashihara N, Matsubara H, Yamasaki Y, Makino H.** Overexpression of angiotensin type 2 receptor ameliorates glomerular injury in mouse remnant kidney model. *Am J Physiol Renal Physiol* 286: F516–F525, 2004.
16. **Heishi T, Hosaka T, Suzuki Y, Miyashita H, Oike Y, Takahashi T, Nakamura T, Arioka S, Mitsuda Y, Takakura T, Hojo K, Matsumoto M, Yamauchi C, Ohta H, Sonoda H, Sato Y.** Endogenous angiogenesis inhibitor vasohibin1 exhibits broad-spectrum antilymphangiogenic activity and suppresses lymph node metastasis. *Am J Pathol* 176: 1950–1958, 2010.
17. **Ichinose K, Maeshima Y, Yamamoto Y, Kinomura M, Hirokoshi K, Kitayama H, Takazawa Y, Sugiyama H, Yamasaki Y, Agata N, Makino H.** 2-(8-Hydroxy-6-methoxy-1-oxo-1h-2-benzopyran-3-yl) propionic acid, an inhibitor of angiogenesis, ameliorates renal alterations in obese type 2 diabetic mice. *Diabetes* 55: 1232–1242, 2006.
18. **Ichinose K, Maeshima Y, Yamamoto Y, Kitayama H, Takazawa Y, Hirokoshi K, Sugiyama H, Yamasaki Y, Eguchi K, Makino H.** Anti-angiogenic endostatin peptide ameliorates renal alterations in the early stage of type 1 diabetic nephropathy model. *Diabetes* 54: 2891–2903, 2005.
19. **Kanegae Y, Lee G, Sato Y, Tanaka M, Nakai M, Sakaki T, Sugano S, Saito I.** Efficient gene activation in mammalian cells by using recombinant adenovirus expressing site-specific Cre recombinase. *Nucleic Acids Res* 23: 3816–3821, 1995.
20. **Kosugi T, Nakayama T, Li Q, Chiodo VA, Zhang L, Campbell-Thompson M, Grant M, Croker BP, Nakagawa T.** Soluble Flt-1 gene therapy ameliorates albuminuria but accelerates tubulointerstitial injury in diabetic mice. *Am J Physiol Renal Physiol* 298: F609–F616, 2010.
21. **Ku CH, White KE, Dei Cas A, Hayward A, Webster Z, Bilous R, Marshall S, Viberti G, Gnudi L.** Inducible overexpression of sFlt-1 in podocytes ameliorates glomerulopathy in diabetic mice. *Diabetes* 57: 2824–2833, 2008.
22. **Li Y, Kang YS, Dai C, Kiss LP, Wen X, Liu Y.** Epithelial-to-mesenchymal transition is a potential pathway leading to podocyte dysfunction and proteinuria. *Am J Pathol* 172: 299–308, 2008.
23. **Lindenmeyer MT, Kretzler M, Boucherot A, Berra S, Yasuda Y, Henger A, Eichinger F, Gaiser S, Schmid H, Rastaldi MP, Schrier RW, Schlondorff D, Cohen CD.** Interstitial vascular rarefaction and reduced VEGF-A expression in human diabetic nephropathy. *J Am Soc Nephrol* 18: 1765–1776, 2007.
24. **Macconi D, Ghilardi M, Bonassi ME, Mohamed EI, Abbate M, Colombi F, Remuzzi G, Remuzzi A.** Effect of angiotensin-converting enzyme inhibition on glomerular basement membrane permeability and distribution of zonula occludens-1 in MWF rats. *J Am Soc Nephrol* 11: 477–489, 2000.
25. **Maeshima Y, Makino H.** Angiogenesis and chronic kidney disease. *Fibrogenesis Tissue Repair* 3: 13, 2010.
26. **Maeshima Y, Sudhakar A, Lively JC, Ueki K, Kharbanda S, Kahn CR, Sonenberg N, Hynes RO, Kalluri R.** Tumstatin, an endothelial cell-specific inhibitor of protein synthesis. *Science* 295: 140–143, 2002.
27. **Makino H, Kashihara N, Sugiyama H, Kanao K, Sekikawa T, Okamoto K, Maeshima Y, Ota Z, Nagai R.** Phenotypic modulation of the mesangium reflected by contractile proteins in diabetes. *Diabetes* 45: 488–495, 1996.
28. **Nangaku M.** Chronic hypoxia and tubulointerstitial injury: a final common pathway to end-stage renal failure. *J Am Soc Nephrol* 17: 17–25, 2006.
29. **Nasu T, Maeshima Y, Kinomura M, Hirokoshi-Kawahara K, Tanabe K, Sugiyama H, Sonoda H, Sato Y, Makino H.** Vasohibin-1, a negative feedback regulator of angiogenesis, ameliorates renal alterations in a mouse model of diabetic nephropathy. *Diabetes* 58: 2365–2375, 2009.
30. **Nyengaard JR, Rasch R.** The impact of experimental diabetes mellitus in rats on glomerular capillary number and sizes. *Diabetologia* 36: 189–194, 1993.
31. **Okada S, Shikata K, Matsuda M, Ogawa D, Usui H, Kido Y, Nagase R, Wada J, Shikata Y, Makino H.** Intercellular adhesion molecule-1-deficient mice are resistant against renal injury after induction of diabetes. *Diabetes* 52: 2586–2593, 2003.
32. **Sassy-Prigent C, Heudes D, Mandet C, Belair MF, Michel O, Perdereau B, Bariety J, Bruneval P.** Early glomerular macrophage recruitment in streptozotocin-induced diabetic rats. *Diabetes* 49: 466–475, 2000.
33. **Sato W, Kosugi T, Zhang L, Roncal CA, Heinig M, Campbell-Thompson M, Yuzawa Y, Atkinson MA, Grant MB, Croker BP, Nakagawa T.** The pivotal role of VEGF on glomerular macrophage infiltration in advanced diabetic nephropathy. *Lab Invest* 88: 949–961, 2008.
34. **Senthil D, Choudhury GG, McLaurin C, Kasinath BS.** Vascular endothelial growth factor induces protein synthesis in renal epithelial cells: a potential role in diabetic nephropathy. *Kidney Int* 64: 468–479, 2003.
35. **Sharma K, Jin Y, Guo J, Ziyadeh FN.** Neutralization of TGF-beta by anti-TGF-beta antibody attenuates kidney hypertrophy and the enhanced extracellular matrix gene expression in STZ-induced diabetic mice. *Diabetes* 45: 522–530, 1996.
36. **Sharma K, Ziyadeh FN.** Hyperglycemia and diabetic kidney disease. The case for transforming growth factor-beta as a key mediator. *Diabetes* 44: 1139–1146, 1995.
37. **Shen J, Yang X, Xiao WH, Hackett SF, Sato Y, Campochiaro PA.** Vasohibin is up-regulated by VEGF in the retina and suppresses VEGF receptor 2 and retinal neovascularization. *FASEB J* 20: 723–725, 2006.
38. **Sung SH, Ziyadeh FN, Wang A, Pyagay PE, Kanwar YS, Chen S.** Blockade of vascular endothelial growth factor signaling ameliorates diabetic albuminuria in mice. *J Am Soc Nephrol* 17: 3093–3104, 2006.
39. **Suzuki Y, Kobayashi M, Miyashita H, Ohta H, Sonoda H, Sato Y.** Isolation of a small vasohibin-binding protein (SVBP) and its role in vasohibin secretion. *J Cell Sci* 123: 3094–3101, 2010.
40. **Takano Y, Yamauchi K, Hiramatsu N, Kasai A, Hayakawa K, Yokouchi M, Yao J, Kitamura M.** Recovery and maintenance of nephrin expression in cultured podocytes and identification of HGF as a repressor of nephrin. *Am J Physiol Renal Physiol* 292: F1573–F1582, 2007.
41. **Tsuchida K, Makita Z, Yamagishi S, Atsumi T, Miyoshi H, Obara S, Ishida M, Ishikawa S, Yasumura K, Koike T.** Suppression of transforming growth factor beta and vascular endothelial growth factor in diabetic nephropathy in rats by a novel advanced glycation end product inhibitor, OPB-9195. *Diabetologia* 42: 579–588., 1999.
42. **Wada T, Furuichi K, Sakai N, Iwata Y, Yoshimoto K, Shimizu M, Takeda SI, Takasawa K, Yoshimura M, Kida H, Kobayashi KI, Mukaida N, Naito T, Matsushima K, Yokoyama H.** Up-regulation of monocyte chemoattractant protein-1 in tubulointerstitial lesions of human diabetic nephropathy. *Kidney Int* 58: 1492–1499, 2000.
43. **Wang JJ, Zhang SX, Mott R, Chen Y, Knapp RR, Cao W, Ma JX.** Anti-inflammatory effects of pigment epithelium-derived factor in diabetic nephropathy. *Am J Physiol Renal Physiol* 294: F1166–F1173, 2008.
44. **Wang JJ, Zhang SX, Mott R, Knapp RR, Cao W, Lau K, Ma JX.** Salutary effect of pigment epithelium-derived factor in diabetic nephropathy: evidence for antifibrogenic activities. *Diabetes* 55: 1678–1685, 2006.
45. **Watanabe K, Hasegawa Y, Yamashita H, Shimizu K, Ding Y, Abe M, Ohta H, Imagawa K, Hojo K, Maki H, Sonoda H, Sato Y.** Vasohibin as an endothelium-derived negative feedback regulator of angiogenesis. *J Clin Invest* 114: 898–907, 2004.
46. **Weibel ER.** Stereological methods. In: *Practical Methods for Biological Morphometry*. London, UK: Academic, 1979, p. 51–57.
47. **Yamaguchi Y, Iwano M, Suzuki D, Nakatani K, Kimura K, Harada K, Kubo A, Akai Y, Toyoda M, Kanauchi M, Neilson EG, Saito Y.** Epithelial-mesenchymal transition as a potential explanation for podocyte depletion in diabetic nephropathy. *Am J Kidney Dis* 54: 653–664, 2009.
48. **Yamamoto Y, Maeshima Y, Kitayama H, Kitamura S, Takazawa Y, Sugiyama H, Yamasaki Y, Makino H.** Tumstatin peptide, an inhibitor of angiogenesis, prevents glomerular hypertrophy in the early stage of diabetic nephropathy. *Diabetes* 53: 1831–1840, 2004.
49. **Yamashita H, Abe M, Watanabe K, Shimizu K, Moriya T, Sato A, Satomi S, Ohta H, Sonoda H, Sato Y.** Vasohibin prevents arterial neointimal formation through angiogenesis inhibition. *Biochem Biophys Res Commun* 345: 919–925, 2006.
50. **Zhang SX, Wang JJ, Lu K, Mott R, Longeras R, Ma JX.** Therapeutic potential of angiostatin in diabetic nephropathy. *J Am Soc Nephrol* 17: 475–486, 2006.

Clinical and Functional Characterization of URAT1 Variants

Velibor Tasic[1], Ann Marie Hynes[2], Kenichiro Kitamura[3], Hae Il Cheong[4], Vladimir J. Lozanovski[1], Zoran Gucev[1], Promsuk Jutabha[5], Naohiko Anzai[5], John A. Sayer[2]*

1 Medical School, University Children's Hospital, Skopje, Macedonia, **2** Institute of Genetic Medicine, Newcastle University, Central Parkway, Newcastle upon Tyne, United Kingdom, **3** Department of Nephrology, Kumamoto University Graduate School of Life Sciences, Kumamoto, Japan, **4** Department of Pediatrics, Seoul National University Children's Hospital, Seoul, Korea, **5** Department of Pharmacology and Toxicology, Dokkyo Medical University School of Medicine, Mibu, Tochigi, Japan

Abstract

Idiopathic renal hypouricaemia is an inherited form of hypouricaemia, associated with abnormal renal handling of uric acid. There is excessive urinary wasting of uric acid resulting in hypouricaemia. Patients may be asymptomatic, but the persistent urinary abnormalities may manifest as renal stone disease, and hypouricaemia may manifest as exercise induced acute kidney injury. Here we have identified Macedonian and British patients with hypouricaemia, who presented with a variety of renal symptoms and signs including renal stone disease, hematuria, pyelonephritis and nephrocalcinosis. We have identified heterozygous missense mutations in *SLC22A12* encoding the urate transporter protein URAT1 and correlate these genetic findings with functional characterization. Urate handling was determined using uptake experiments in HEK293 cells. This data highlights the importance of the URAT1 renal urate transporter in determining serum urate concentrations and the clinical phenotypes, including nephrolithiasis, that should prompt the clinician to suspect an inherited form of renal hypouricaemia.

Citation: Tasic V, Hynes AM, Kitamura K, Cheong HI, Lozanovski VJ, et al. (2011) Clinical and Functional Characterization of URAT1 Variants. PLoS ONE 6(12): e28641. doi:10.1371/journal.pone.0028641

Editor: Shree Ram Singh, National Cancer Institute, United States of America

Received September 5, 2011; **Accepted** November 11, 2011; **Published** December 16, 2011

Funding: This work was supported in part by grants from the Japan Society for the Promotion of Science (JSPS KAKENHI 21390073, 21659216, 21890245), the Nakatomi Foundation, and Gout Research Foundation of Japan (NA, PJ). This study was partly supported by a grant of the Korea Healthcare technology R&D Project, Ministry for Health, Welfare and Family Affairs, Republic of Korea (A080588)(HIC). AMH is supported by Newcastle Healthcare Charities and the Northern Counties Kidney Research Fund, UK. JAS is a GlaxoSmithKline clinician scientist. The funders had no role in study design, data collection and analysis, decision to publish or preparation of the manuscript.

Competing Interests: The authors have read the journal's policy and have the following conflicts: JAS is a GlaxoSmithKline clinician scientist. This does not alter the authors' adherence to all the PLoS ONE policies on sharing data and materials.

* E-mail: j.a.sayer@ncl.ac.uk

Introduction

In man, the level of serum uric acid is determined primarily by the production of urate, as an end product of purine metabolism (for which the liver enzyme xanthine oxidase is necessary) versus biliary and urinary tract elimination. In the majority of other mammals, uric acid is metabolized by uricase (urate oxidase) to allantoin, before urinary excretion. Thus man (and other species lacking uricase, such as great apes), has comparably higher serum uric acid levels than most mammals.

The renal handling of uric acid is a complex and incompletely understood process [1,2]. Uric acid is freely filtered at the glomerulus, the majority undergoes reabsorption via proximal tubular urate transporter proteins and a proportion (~10%) is secreted back into the filtrate in the late proximal tubule. Molecular genetic and genome wide association studies have recently allowed the identification of several proximal tubule urate transporters including URAT1 (alias SLC22A12) [3] and GLUT9 (alias SLC2A9) [4,5,6]. Proposed models of urate transport in the proximal tubule [7] suggest an initial uptake of uric acid from the filtrate by URAT1, coupled to organic acid transporters. GLUT9, in two different isoforms, allows for basolateral exit of urate from the proximal tubule (isoform I) and regulation of urate entry/exit at the apical membrane (GLUT9ΔN isoform). Finally, in the late proximal tubule there are transporter proteins mediating uric acid secretion (including ABCG2, NPT1 and NPT4) [7]. As uric acid excretion is mediated through molecular transporters, certain drugs such as fenofibrate, valproic acid, trimethoprim and losartan may be used to manipulate these processes [8,9,10], thus allowing manipulation of serum uric acid levels.

In humans, genetic defects in the activity of xanthine oxidase or an acquired defect in liver enzyme function or renal uric acid handling may result in hypouricaemia. Acquired hypouricaemia may be seen in a number of clinical disorders, including Fanconi syndrome [11], type 1 and type 2 diabetes mellitus [12,13], thyrotoxicosis [14], pseudohypoparathyroidism type 1b [15], pseudoaldosteronism due to licorice ingestion [16], distal renal tubular acidosis [17,18], obstructive jaundice [19] and severe acute respiratory syndrome [20].

Idiopathic renal hypouricaemia is an inherited form of hypouricaemia that is characterized by excessive urinary wasting of uric acid leading to an increased clearance (and increased fractional excretion) of uric acid. The majority of patients are asymptomatic, but some may present with uric acid nephrolithiasis or acute kidney injury following severe exercise [21]. In 2002, Enomoto *et al.* reported that mutations in gene *SLC22A12* encoding the URAT1 transporter were responsible for most cases of idiopathic renal hypouricaemia [3]. Recently Anzai et al. found

mutations in *SLC2A9*, encoding GLUT9, in patients with severe renal hypouricaemia [22]. It is noteworthy that reports of idiopathic renal hypouricaemia secondary to mutations in uric acid transporters URAT1 and GLUT9 were initially reported from Japan, Korea and China [23]. More recently, three Jewish Israeli families of Iraqi origin have been reported to have renal hypouricaemia, with a common mutation in *SLC22A12* [24]. Inactivating mutations in *SLC22A12* have not yet, to our knowledge, been reported in a Caucasian population.

The typical presentation of idiopathic renal hypouricaemia is that of exercise induced acute kidney injury with a preceding history of loin pain with nausea and vomiting for several hours after physical exercise. The exact mechanism of renal damage is unclear, but may relate to damage from oxygen free radicals [21]. In contrast to this dramatic presentation, most patients are well with no overt clinical symptoms, although renal stones and hematuria may be presenting symptoms and signs.

Here we present data from Skopje (Macedonia) and Newcastle upon Tyne (UK) where we have investigated the underlying genetic cause of hypouricaemia in patients of European descent. We present mutations in *SLC22A12* encoding URAT1 alongside their clinical, biochemical and functional characterization. This data highlights the importance of renal urate transporters in determining serum urate concentrations, and the clinical phenotypes that should lead the renal clinician to suspect an inherited form of renal hypouricaemia.

Results

Clinical descriptions

A total of thirty two patients with hypouricaemia were recruited (Macedonia, n = 20 and United Kingdom n = 12) for mutational analysis of the *SLC22A12* and *SLC2A9* genes. The basic demographic, clinical, laboratory and molecular genetic data from these patients are given in Table 1. We found changes in *SLC22A12* in five patients from Macedonia and two patients from the United Kingdom (Figure 1A). No pathogenic mutations in *SLC2A9* were identified. An outline of the clinical, biochemical and molecular genetic features of each case is given below.

Patient SK-1: This 7 year old girl was referred to the nephrology unit with persistent vomiting, presumed to be secondary to a non-obstructive kidney stone. She had a history of similar episodes during the preceding 6 months. On admission she was alert, but pale and moderately dehydrated. Clinical examination revealed that her abdomen was non-tender with no renal masses. A renal ultrasound scan (USS) revealed a single stone within the right kidney measuring 10 mm, without calyceal dilatation. Laboratory investigations on admission revealed normal renal function (serum creatinine 26 μmol/l, estimated glomerular filtration rate 123 ml/min/1.73 m^2 (according to Schwartz formula)). Although she was moderately dehydrated, she had persistently low serum uric acid levels ranging from 0.72–1.18 mg/dl. FE_{urate} was elevated at 20.8%. Liver function tests, serum electrolytes, total protein and albumin were within reference values. Urinary excretion of cystine, calcium, phosphate, oxalate, glucose, low molecular weight proteins, amino acids and organic acids were also within reference limits. In order to clarify the etiology of urolithiasis, urinary excretion of xanthine and hypoxanthine was measured, showing normal values. Mutation analysis of *SLC22A12* revealed a heterozygous missense mutation, leading to amino acid change p.R434C. Genetic screening of other family members revealed that her brother and father both carried the identical heterozygous change, but were asymptomatic in terms of renal stones, with normal renal ultrasound scan and no reported episodes of exercise induced renal failure. Biochemical evaluation revealed that the father had normal values of serum uric acid while the brother had moderately decreased serum uric acid level (1.56 mg/dl).

Patient SK-2: This 18 year female was referred for management of hypertension. She had a past medical history of pyelonephritis and bilateral ureteric reflux with scarring of the left kidney, as determined by USS and Tc^{99}DMSA scan. Laboratory investigations revealed serum creatinine and urea within normal limits. She was found to have low serum uric acid levels on two occasions (1.74 mg/dl and 1.78 mg/dl, respectively) with an increased FE_{urate}. She had mild proteinuria (0.35 g/24 h) and a renal USS revealed a small left kidney, but no evidence of nephrolithiasis. Mutational analysis of the *SLC22A12* gene was performed and a heterozygous missense mutation p.R434H was detected.

Patient SK-3: This 5 year old girl was admitted to the nephrology unit with severe dehydration, polyuria and vomiting. She was noted to have faltering growth and rickets. Laboratory investigations revealed a hyperchloremic metabolic acidosis (pH 7.23, HCO_3 13.6 mmol/l, BE −12.6 mmol/l), hypokalemia (3.0 mmol/l), hypophosphatemia (0.84 mmol/l) and hypouricaemia (1.24 mg/dl). Simultaneous measurement of urine pH with electrode revealed value of 6.77 which pointed to distal acidification defect (expected urine pH<5.5). There was evidence of proteinuria on urine dipstix testing (1+) which was characterized with SDS-PAG electrophoresis as complete tubular proteinuria. There was a generalized hyperaminoaciduria, but no glucosuria. There was also evidence of uricosuria (FE_{urate} varied between 24–

Table 1. Demographic, clinical, biochemical and molecular genetic data on 6 patients with renal hypouricaemia.

Patient	Age (yrs)	Sex	Serum Urate (mg/dl)	FE_{urate} (%)	Renal symptoms*	Comorbidity	URAT1 mutation leading to missense
SK-1	7	F	0.72	21	Nephrolithiasis	Cyclic vomiting	p.R434C
SK-2	18	F	1.75	27	Previous pyelonephritis	Reflux nephropathy; Hypertension	p.R434H
SK-3	5.5	F	1.24	31	Nephrocalcinosis	Distal renal tubular acidosis	p.R434C
SK-4	8	M	1.24	27	Recurrent episodes of gross hematuria and renal colic	Alport syndrome	p.R347S
SK-5	7	F	1.28	17	None	Hashimoto thyroiditis; vitiligo	p.R434H
NC-1	41	F	2.00 (transient)	16	Recurrent nephrolithiasis	Type I diabetes mellitus; hypothyroidism	p.V388M
NC-2	45	F	2.02	N/A	Recurrent nephrolithiasis	None	p.I75T

*Symptoms due to renal hypouricaemia, SK-Skopje, NC-Newcastle, FE_{urate}- Fractional excretion of uric acid, N/A- not available.

doi:10.1371/journal.pone.0028641.t001